KLOE Note n° 187

April 2003

Measuring the branching ratio of the $K^{\pm} \to \pi^{\pm}\pi^{0}\pi^{0}$ decay

E.Gorini[a,b], **M.Primavera**[b], **A.Ventura**[a,b]

[a] *Dipartimento di Fisica - Università degli Studi di Lecce*

[b] *Sezione INFN - Lecce*

Abstract

A measurement of the branching ratio of the $K^{\pm} \to \pi^{\pm}\pi^{0}\pi^{0}$ decay is presented, based on a sample of 441 pb^{-1} of the KLOE data collected during years 2001 and 2002. A detailed description of the selection algorithm, the various efficiencies involved in the analysis and, finally, the systematic uncertainties, is given. To perform the measurement two independent tagging strategies are applied and the final results are combined.

Contents

Document ID	$\Gamma(\pi^{\pm}\pi^0\pi^0)/\Gamma_{total}$ $(\cdot 10^{-2})$	Events
Chiang 72 [9]	1.84 ± 0.06	1307
Pandoulas 70 [8]	1.53 ± 0.11	198
Shaklee 64 [7]	1.8 ± 0.2	108
Roe 61 [6]	1.7 ± 0.2	
Taylor 59 [5]	1.5 ± 0.2	
Alexander 57 [4]	2.2 ± 0.4	
Birge 56 [3]	2.1 ± 0.5	

Table 1: Experimental measurements of the branching ratio of τ'. Only the first four results in the table are used by PDG [2] for the fit.

1 Introduction

1.1 Motivations of the measurement

The $K^{\pm} \rightarrow \pi^{\pm}\pi^0\pi^0$ decay mode, also indicated as τ', represents a very interesting process for testing the direct $\mathcal{CP}$ asimmetry [1], since no oscillation is allowed by charge conservation and $\mathcal{CP}$ violation can occur through the direct mode only.

The experimental measurements of the τ' branching ratio which are considered by Particle Data Group [2] are listed in Tab. 1. Only the first four measurements enter in the PDG world fit, which provides:

$$BR(\tau') = (1.73 \pm 0.04) \cdot 10^{-2} \ . \tag{1.1}$$

As can be observed, all the measurements date back to more than thirty years ago and are characterized by large relative errors (3.5% in the most precise experiment). Moreover, they have been performed on samples which contained only positive kaons, so that no information was reached about possible asymmetries in the K^+ and the K^- decay rates and consequent tests of $\mathcal{CP}$ simmetry conservation.

KLOE can perform a new and significantly more precise measurement of this branching ratio. Given the large amount of data and keeping systematics under control, a total accuracy of $\sim 1\%$ can be reached.

1.2 Applied method

In the present analysis τ' decays are tagged by "K_θ" and "K_μ" decays, *i.e.* they are searched in events in which a $K^{\pm} \rightarrow \pi^{\pm}\pi^0$ or a $K^{\pm} \rightarrow \mu^{\pm}\nu_\mu$ decay is observed, respectively. The K_θ-tag events [1] are defined in such a way that the *tag-hemisphere*

[1]The scheme described here for K_θ-tag decays is also applied for the K_μ-tag, with the obvious change of notation $\theta \rightarrow \mu$.

provide the trigger ("K_θ-*selftag*") and the classification of the event.

Let $\epsilon^{\tau'}_{tag\theta}$ be the efficiency to select a K_θ-tag when in the opposite hemisphere there is a signal event (see sections 2.2 and 2.3) and $\epsilon^{\tau'}_{\theta sel}$ the efficiency of the selection algorithm to recognize a τ' decay given the K_θ-tag (see Sect. 3): the final number of selected τ' events is

$$N^{\tau'}_{tag\theta} = N^{\tau'}_{true} \cdot BR(K^\pm \to \pi^\pm\pi^0) \cdot \epsilon^{\tau'}_{tag\theta} \cdot \epsilon^{\tau'}_{\theta sel} \ . \tag{1.2}$$

The efficiency $\epsilon^{\tau'}_{tag\theta}$ can be factorized as:

$$\epsilon^{\tau'}_{tag\theta} = \epsilon_{trig} \cdot \epsilon_{EvCl} \cdot \epsilon^{\tau'}_{CV} \cdot \epsilon^{\tau'}_{FILFO} \cdot \epsilon^{\tau'}_{\theta} \ , \tag{1.3}$$

where:

- ϵ_{trig} is the trigger [12] efficiency;
- ϵ_{EvCl} is the efficiency of the event classification algorithm [13, 14];
- $\epsilon^{\tau'}_{CV}$ is the efficiency of the cosmic-ray trigger veto [15] in τ' events;
- $\epsilon^{\tau'}_{FILFO}$ is the efficiency of the FILFO machine background rejection algorithm [16] in τ' events;
- $\epsilon^{\tau'}_{\theta}$ is the efficiency of the tagging selection in τ' events.

The branching ratio of τ' can be defined as:

$$BR(K^\pm \to \pi^\pm\pi^0\pi^0) = \frac{N^{\tau'}_{true}}{N^{\theta}_{true}} \cdot BR(K^\pm \to \pi^\pm\pi^0) \tag{1.4}$$

where N^{θ}_{true} is the number of truly produced K_θ's, related to the number of finally selected K_θ decays, $N_{tag\theta}$, by the relation:

$$N_{tag\theta} = N^{\theta}_{true} \cdot \epsilon_{tag\theta} \ . \tag{1.5}$$

The efficiency $\epsilon_{tag\theta}$ can be expressed as

$$\epsilon_{tag\theta} = \epsilon_{trig} \cdot \epsilon_{EvCl} \cdot \epsilon^{\theta}_{CV} \cdot \epsilon^{\theta}_{FILFO} \cdot \epsilon_{\theta} \ , \tag{1.6}$$

where ϵ^{θ}_{CV}, $\epsilon^{\theta}_{FILFO}$ and ϵ_θ are defined as previously, but independently of the decay mode in the non-tag hemisphere, while ϵ_{trig} and ϵ_{EvCl} are exactly the same as in equation (1.3) and then cancel out in the ratio [2].

The branching ratio (1.4) then becomes:

$$BR(\tau') = \frac{N^{\tau'}_{tag\theta}}{N_{tag\theta}} \cdot \frac{1-\xi^{\tau'}_{bckg}}{1-\xi^{\theta}_{bckg}} \cdot \frac{1}{\epsilon^{\tau'}_{\theta sel}} \cdot \frac{1}{[BR(\pi^0 \to \gamma\gamma)]^2} \cdot \left[\frac{\epsilon^{\theta}_{CV}\ \epsilon^{\theta}_{FILFO}\ \epsilon_{\theta}}{\epsilon^{\tau'}_{CV}\ \epsilon^{\tau'}_{FILFO}\ \epsilon^{\tau'}_{\theta}}\right] \ . \tag{1.7}$$

[2]This comes directly from the preliminary requirement of a *self-tag* in the event.

In equation (1.7) ξ^{θ}_{bckg} and $\xi^{\tau'}_{bckg}$ are, respectively, the background fraction in the K_θ-tag and in the τ' signal; they are determined through MC and corrected on data as shown in Sect. 4.

The term $BR(\pi^0 \to \gamma\gamma)$, known to be $(98.798 \pm 0.032)\%$ [2], is introduced since in the whole analysis the identification of neutral pions is performed by looking for $\pi^0 \to \gamma\gamma$ decays [3] . As a consequence, $\epsilon^{\tau'}_{\theta sel}$ is redefined as the efficiency to select τ' decays in $\pi^\pm 4\gamma$ final state and is expressed as factorization of different terms, as described in Sect. 5. Each term is estimated directly from data by means of suitable samples of events.

Finally, the ratio in square brackets is studied and discussed in detail in Sect. 6 together with the systematics on $\epsilon^{\tau'}_{sel\theta}$.

1.3 Data and Monte Carlo samples

Data collected during 2001 and 2002 KLOE running periods have been used, processed and filtered by the official reconstruction software [18, 19] and the event classification algorithms [13, 14]. Both the signal and all the data subsamples necessary for the evaluation of the efficiencies involved in the analysis have been selected from the "*kpmstream*".

The whole amount of analyzed data corresponds to an integrated luminosity of 441 pb^{-1}, which corresponds to the KLOE collected statistics during the period from March 2001 and September 2002. It has been divided in 4 different subsamples, referred to as A, B, C and D (see Tab. 2). The choice of working with samples of different size is the result of an optimization, which aims to study separately the final sample from those used for the efficiencies, while minimizing the total statistical error. Each of the four samples is composed in such a manner to represent uniformly the whole data set with respect to the running period; this has been done in order to control the stability of the detector and selection performance. The analyzed data sample is enough to reach a total statistical accuracy of 0.7 %, including the contribution from the control samples used for the efficiencies, while the overall systematic error on the measurement prevails.

Monte Carlo has been used in this analysis to help in the choice of the selection criteria and to estimate background. It has been generated by the official KLOE Monte Carlo package, [20, 21]. The same version of the reconstruction software has been used for real data and Monte Carlo, but including in this last case the simulation [22, 23] of electronic noise and unphysical background to the electromagnetic calorimeter (EMC) and to the drift chamber (DC) according to the typical rates/configurations observed in the data.

[3] The occurrence of π^0 Dalitz decays yields 4-track vertices in K_θ and 4-track (or even 6-track) vertices in τ' decays, which can be easily misidentified as $K^\pm \to \pi^\pm\pi^+\pi^-$: since the KLOE vertexing algorithm [17] is not specifically optimized for reconstructing vertices with high track multiplicity, π^0 Dalitz decays have been ignored.

Sample	$\int \mathcal{L} dt$
Sample A	187 pb^{-1}
Sample B	173 pb^{-1}
Sample C	50.8 pb^{-1}
Sample D	29.8 pb^{-1}

Table 2: Data samples collected at KLOE and used in this analysis.

Three different MC samples have been generated and reconstructed as explained above:

- Events in which the ϕ meson decays in its main modes (K^+K^-, K_SK_L, $\rho\pi$, $\pi^+\pi^-\pi^0$, $\eta\gamma$) and the charged kaons decay in their six main modes ($\mu^\pm\nu$, $\pi^\pm\pi^0$, $\pi^\pm\pi^+\pi^-$, $e^\pm\pi^0\nu$, $\mu^\pm\pi^0\nu$ and $\pi^\pm\pi^0\pi^0$) (**ALLPHI**, corresponding to 5 pb^{-1}).
- $\phi \to K^+K^-$ events with $K^\pm \to \pi^\pm\pi^0\pi^0$ and $K^\mp \to$ all allowed modes (**PP0P0**, corresponding to 60 pb^{-1}).
- $\phi \to K^+K^-$ events with $K^\pm \to l^\pm\pi^0\pi^0\nu_l$ ($l = e, \mu$) and $K^\mp \to$ all allowed modes (**LP0P0NU**, corresponding to 2 fb^{-1}).

2 Selection of the self-triggering tag events

The main advantages in tagging K^+K^- events by means of K_θ or K_μ decays are the high statistics (about 85% of all the $K^\pm$'s decay in these modes) and the fact that, since they are two-body decays, the $\pi^\pm/\mu^\pm$ daughter track has a well-defined momentum in the kaon rest frame that can be easily identified. The $K \to \mu\nu$ decay is characterized by the larger branching ratio, but the $K \to \pi\pi^0$ mode is favoured to self-trigger an event.

As already mentioned in Sect. 1.2, the tagging strategy allows to simplify in the branching ratio two following contributions:

- ϵ_{EvCl}: efficiency for the Event Classification algorithms to filter a K^+K^- event with a K_θ (or K_μ) decay, assuming that such efficiency is a function of the single charged kaon in the K^+K^- event. This assumption corresponds to require **only events filtered in the analysis by the** *kpmfilt* **algorithm 5**, since this algorithm considers the two kaons as uncorrelated.
- ϵ_{trig}: efficiency that the filtered events have been triggered by the particles directly involved in the tag.

2.1 Preliminary requirements on the 2-track vertex

The search for a K_θ or a K_μ decay requires a 2-track vertex in the drift chamber volume:

$$\bullet) \qquad \sqrt{x_V^2 + y_V^2} > 25\ cm\ , \tag{2.1}$$

made of a charged kaon track as given by the event classification and a *daughter* track with the same charge.

Since only one charged particle is produced in about 95% of the $K^\pm$ decays the 2-track vertices represent almost the totality of the vertices connected to $K^\pm$'s.

All vertices done with a "backward reconstructed" charged kaon and with the other kaon in the opposite hemisphere (or with a charged particle coming from it) are rejected by applying a cut on the extrapolation length from the last (first) hit of the mother (daughter) track to the vertex V:

$$\bullet) \qquad max\{d(K^\pm_{LH}, V), d(\pi^\pm_{FH}, V)\} < 50\ cm\ . \tag{2.2}$$

The distance of 50 *cm* has been chosen as the diameter of the inner cylinder of the drift chamber.

2.2 The K_θ-tag

In a $K^\pm \to \pi^\pm\pi^0$ decay at KLOE, if the kaon reaches the DC volume, two charged tracks joining in a vertex are expected in the chamber and three clusters have to be found in the calorimeter (two neutral clusters from the $\pi^0 \to \gamma\gamma$ decay and one from the $\pi^\pm$ or from the charged particle coming out from the $\pi/\mu/e$ chain.

2.2.1 Daughter track momentum

The charged pion coming out from the a $K^\pm \to \pi^\pm\pi^0$ vertex has a momentum which is fixed to 205 MeV in the $K^\pm$ rest frame.

A distribution of the daughter track momentum p_π in the $K^\pm$ rest frame is shown in Fig. 1 after the preliminary requirements (2.1) and (2.2). The two peaks correspond to the two 2-body decay modes: $K \to \pi\pi^0$ at $\sim 205\ MeV$ and $K \to \mu\nu$ at $\sim 236\ MeV$. The $\mu\nu$ peak is not centered at the right value and is distorted by the wrong mass hypothesis. The shape of the spectrum at lower momenta is mainly due to the semileptonic and the τ' decays.

A gaussian distribution nicely fits the $\pi\pi^0$ peak in Fig. 1, then a kinematical cut is applied [4] for selecting K_θ decays:

$$\bullet) \qquad 200\ MeV < p_\pi < 210\ MeV\ . \tag{2.3}$$

[4] The width of this cut (and similarly for the following ones) has been chosen as 3σ of the corresponding distribution, and has been oppotunely defined for data and MC.

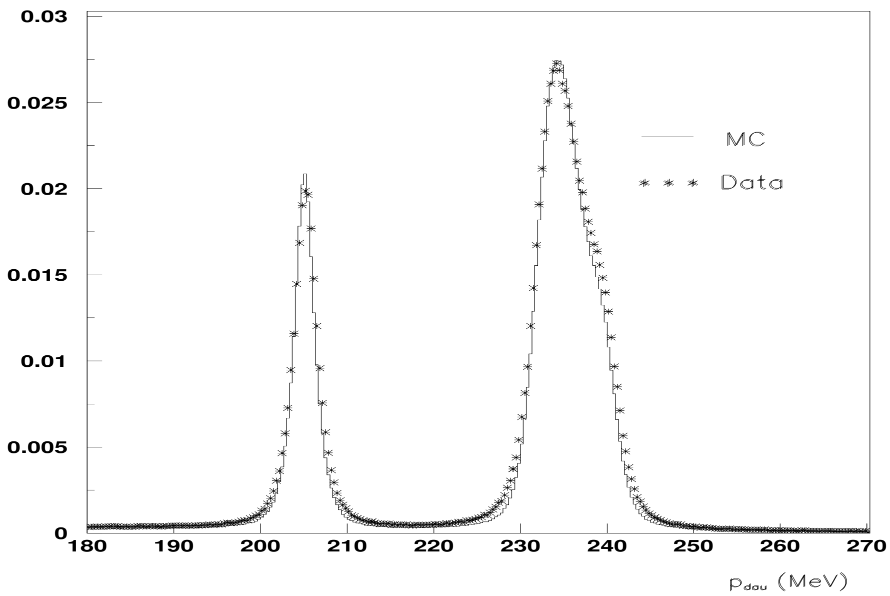

Figure 1: Momentum distribution of the daughter particle (charged pion mass hypothesis) in the $K^{\pm}$ rest frame for data and Monte Carlo events, after the preliminary 2-track vertex selection.

After this cut, the main sources of backgroung are $K \to \mu\nu$ decays and the K_{e3} decays with high momentum $e^{\pm}$. Then, to reduce these contaminations, the missing mass m_m in the vertex has been required to be:

$$\bullet) \qquad 122\ MeV < m_m < 148\ MeV\ . \tag{2.4}$$

In Fig. 2 the distributions of m_m after the cut (2.3) are shown for Monte Carlo (left panel) and for real data (right panel); in the MC plot, the background distribution is superimposed.

The two cuts described above are correlated, but they allow to reach a $\sim 98\%$ purity [5] of the K_θ sample with still no use of EMC variables.

2.2.2 Considerations about clustering

Assuming that the π^0 coming from the $K^{\pm} \to \pi^{\pm}\pi^0$ decay vertex produces two γ's, a pair of neutral (*i.e.* not associated to any reconstructed track [24]) clusters has to be found in the EMC.

For each cluster i reconstructed in the EMC, an energy estimation E_i is assigned, together with an absolute time t_i (depending on the event global time offset t_0^G) and a position vector $\overrightarrow{r}_i$ describing the coordinates of the cluster centroid in the KLOE detector frame. It's important to notice that, **in this analysis no absolute time measurement is used**, and t_i only appear in time differences (*e.g.* $t_i - t_j$),

[5] The "purity" is defined, for a Monte Carlo sample, as the fraction of selected decay vertices in which the $K^{\pm}$ decay mode is the one considered as "signal".

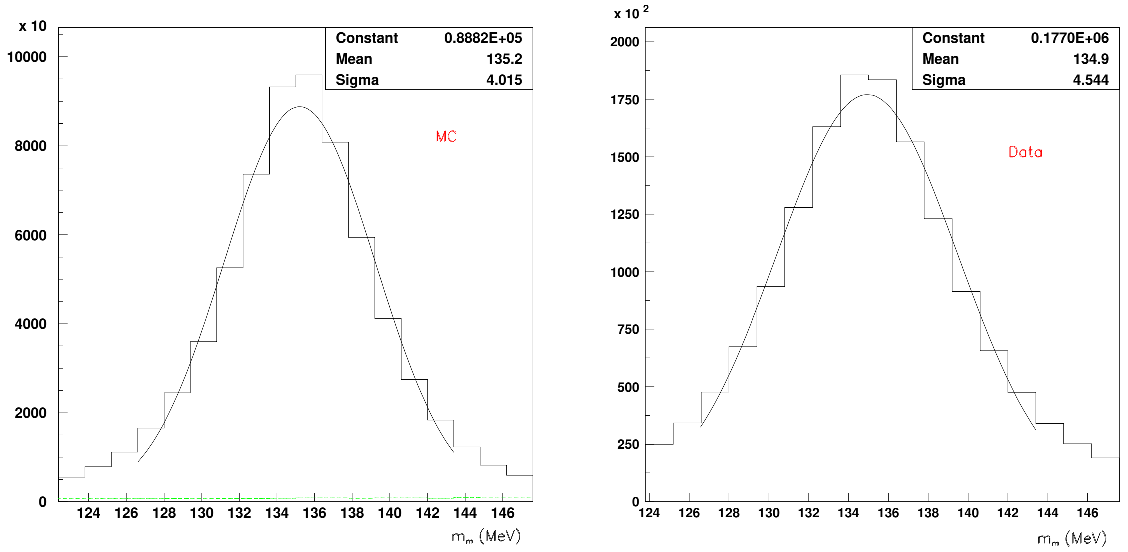

Figure 2: Distributions of the neutral missing mass m_m, after the cut on the daughter track momentum, for MC (left) and for data (right). In the left panel the distribution of the flat background is superimposed.

so that all time offsets in a fixed event cancel out. Getting rid of this source of systematic error is also made possible by the very good time resolution of the KLOE electromagnetic calorimeter [25]

$$\sigma_t(E) = 54\ ps/\sqrt{E(GeV)} \oplus 50\ ps \tag{2.5}$$

which allows a time resolution of less than 300 ps, even for very low energy clusters (down to $20 \div 30\ MeV$).

Actually the time resolution (2.5) for the calorimeter has been evaluated on photons coming out from ϕ radiative decays, which significantly differ from those produced in charged kaons events both for their higher energy range and for their origin vertex. In fact, γ's coming from K^+K^- events can be emitted uniformly in the DC volume, so their time of flight and their passage through the detector materials are quite more complicated to study than the ones for those generated in the origin. Therefore, the spread in time for the clusters can be different from what observed in ϕ decays. A direct estimation of $\sigma_t(E)$ is presented in Sect. 5.2.2, extracted from the $K \to \pi\pi^0$ decay.

Accidental clusters represent the most relevant source of background in reconstructing neutral pions, expecially in the low energy range of $K \to \pi\pi^0$ and τ' decays. Their behaviour in the KLOE EMC has been studied in detail [22]. What concerns the present analysis has mainly two features: (1) these clusters are randomly distributed and not related to physics, so are usually *out of the vertex time* and (2) their energy distribution peaks to rather low values (see the left plot of Fig. 3).

Other background sources on *neutral* clusters are: low-energy cosmic rays that

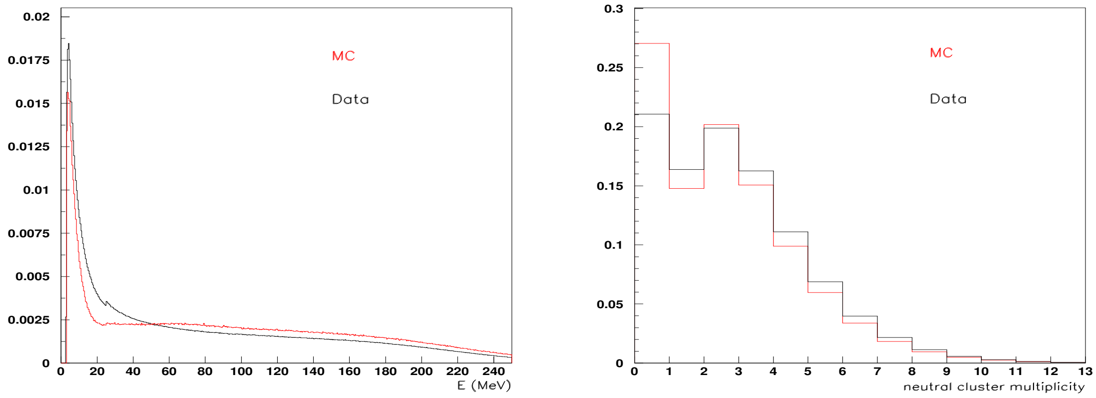

Figure 3: Left: Energy distribution of all the neutral clusters for data and MC. Right: Neutral clusters multiplicity in charged kaons events for data and MC. The MC sample has a lower population of accidentals than the real data.

haven't been rejected at trigger level or inefficiencies in the track-to-cluster algorithm (*e.g.* in the case of clusters due to charged pions/muons impinging on the calorimeter and producing large electromagnetic showers).

Additional neutral clusters due to *splitting*, *i.e.* the fragmentation of the energy deposit of a particle impinging on the EMC, produce a wrong estimation of the position and of the energy of the originary clusters.

Figure 4: Plot of the distances (in cm) of all the possible clusters pairs versus the minimum energy (in MeV) in the pair. The line at 15 MeV refers to the minimum energy cut applied in the analysis.

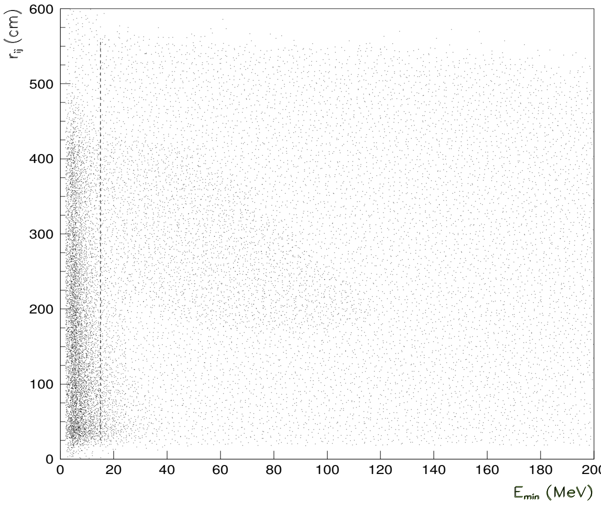

The scatter plot in Fig. 4 shows, for each possible pair of reconstructed clusters in a suitable time window, the tridimensional distance r_{ij} versus the energy E_{min} of the less energetic cluster in the pair. Both data and MC are characterized by a fraction of pairs of short-distanced clusters having a low E_{min}: this is easily explained as a little cluster which has been split from another nearby cluster with higher energy. A "splitting recovery" algorithm is applied before the present analysis, merging pairs of clusters for which

$$r_{ij}(cm) < \frac{r_0}{E_{min}(MeV)} \quad and \quad E_{min} < E_{sup}, \tag{2.6}$$

(where $r_0 = 1000\ cm$ and $E_{sup} = 40\ MeV$) and subsequently redefining times, energies and positions. The algorithm has been analyzed as a possible source of systematic error in the branching ratio (see Sect. 6).

2.2.3 Neutral pion reconstruction

To select a K_θ decay, a cut on the energy of the neutral clusters is performed to reject accidentals or unrecovered splitted clusters:

$$\bullet) \qquad E_i > 15\ MeV\ . \tag{2.7}$$

This cut has been tuned by looking at the energy spectrum of the γ's involved in the $K^\pm$ decays studied in the present analysis.

Then, a fundamental requirement is to find two neutral clusters j and k *on-time* with the vertex V, *i.e.* the time interval defined as

$$\Delta t_{jk} = (t_j - t_k) - \frac{1}{c} \cdot (|\overrightarrow{r}_{Vj}| - |\overrightarrow{r}_{Vk}|) \tag{2.8}$$

has to be near to 0. In equation (2.8) $\overrightarrow{r}_{Vi}$ represents the vector from the vertex point V to the centroid of the cluster i. Since the time resolution depends on the cluster energy, for each possible clusters pair, the on-time condition is required by computing

$$\Delta t'_{jk} = \frac{\Delta t_{jk}}{\sqrt{\sigma_t(E_j)^2 + \sigma_t(E_k)^2}}\ . \tag{2.9}$$

and asking for

$$\bullet) \qquad |\Delta t'_{jk}| < 5\ . \tag{2.10}$$

Accidental clusters surviving the cut on energy that may enter in these pairs of clusters (j, k) are powerfully rejected by applying this cut.

For each selected pair of on-time neutral clusters the condition on the di-photon invariant mass

$$\bullet) \qquad 85\ MeV < m_{\gamma\gamma} < 185\ MeV \tag{2.11}$$

is required and, finally, a cut on the four-momentum conservation in the $K \to \pi\pi^0$ vertex is applied to recognize a K_θ decay:

$$\bullet) \qquad |\Delta P_{\pi\pi^0}| < 50\ MeV \tag{2.12}$$

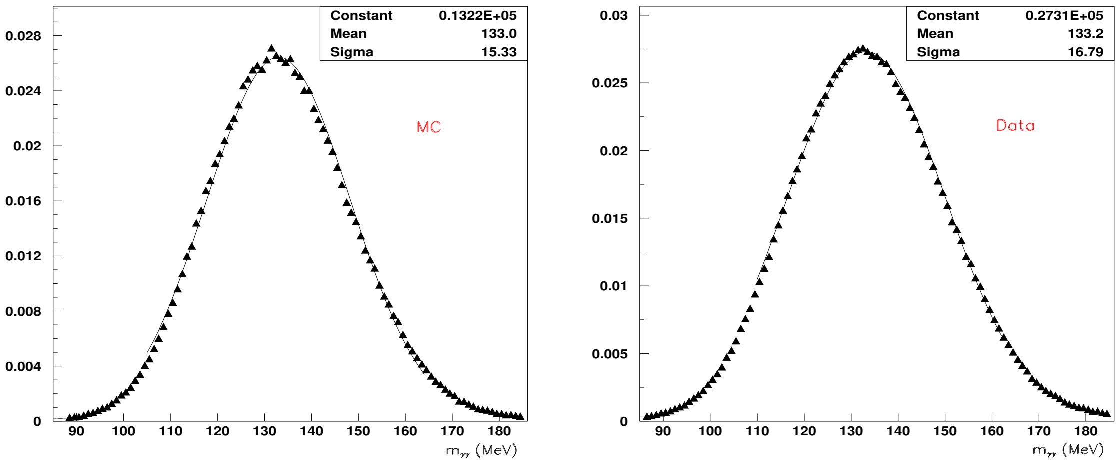

Figure 5: Distributions of the clusters pair invariant mass $m_{\gamma\gamma}$, for MC (left) and for data (right) after the K_θ sample final selection.

where

$$|\Delta P_{\pi\pi^0}|^2 \equiv (E_K - E_D - E_{\gamma\gamma})^2 + |\overrightarrow{p}_K - \overrightarrow{p}_D - \overrightarrow{p}_{\gamma\gamma}|^2 \ .$$

The two plots in Fig. 5 show the distributions of $m_{\gamma\gamma}$ for MC (left) and data (right) K_θ samples; also the results to a gaussian fit in the central region of the plots are reported. The shift in the peak of the distributions with respect to the known π^0 mass [2] originates from the non-optimization of the EMC calibration for low-energy clusters [26], as those involved in this particular analysis; moreover, a non strictly linear response of the calorimeter in the region below 100 MeV can cause a systematic shift of the π^0 mass peak.

2.3 The K_μ-tag

After the preliminary vertex selection (Sect. 2.1), a cut on the daughter track momentum in K rest frame is applied for selecting K_μ decays:

$$\bullet) \qquad 229\ MeV < p_\mu < 241\ MeV \ . \tag{2.13}$$

The main source of background at this level still comes from $K \to \pi\pi^0$ decays and can be efficiently suppressed by requiring

$$\bullet) \qquad |m_m^2| < 5000\ MeV^2 \ . \tag{2.14}$$

on the squared missing mass (see Fig. 6).

2.4 Self-triggering conditions

In order to be triggered by the EMC, in a K_θ or a K_μ candidate event, all the clusters coming from the tagging hemisphere have to satisfy some particular

Figure 6: Distributions of the squared missing mass m_m^2 (expressed in MeV^2), after the cut on the daughter track momentum at the $\mu\nu$ peak, for MC and data.

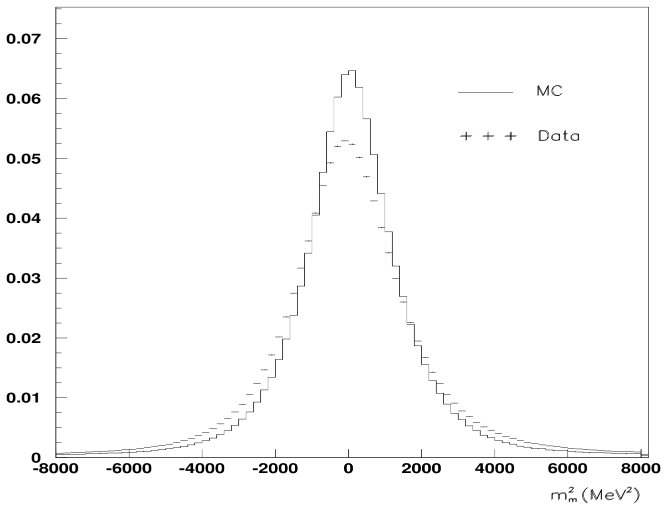

trigger requirements: two energy deposits in two trigger sectors have to overcome a threshold value, which is fixed to 50 MeV in the barrel and 150 MeV in the endcaps.

The most important role for triggering a K_θ event is played by the cluster produced by the charged pion since, when it is successfully reconstructed and associated to the $\pi^\pm$ track, it always reaches the required energy threshold. Then, at least another energy deposit has to be released in the EMC to trigger, so at least one γ cluster has to be over threshold.

The possibility for a K_μ-tag to self-trigger is due to the cluster associated to the daughter $\mu^\pm$ track. The curved trajectory of the $\mu^\pm$ in the magnetic field can sometimes allow for the passage through two adiacent trigger sectors: when this results in two energy deposits over threshold, a K_μ-selftag event is obtained.

These self-triggering conditions are verified in about 90% of the selected K_θ decays and about 35% of the selected K_μ decays. The absolute branching ratio of the τ' decay is computed assuming as normalization the two *selftag* samples described above.

2.5 Background in K_θ and K_μ samples

The relative fraction $\xi^{\theta,\mu}_{bckg}$ of events contaminating tag decays to be subtracted to N_{tag}, has been evaluated both from MC and data.

The contamination in the K_θ sample comes from the other main $K^\pm$ decay modes: (0.307 ± 0.009)%. The occurrence of $\phi \to K_S K_L$ events has been evaluated to be as low as (0.04 ± 0.01)% and other possible channels are negligible, expecially for the very specific requirement (2.3).

A small Bhabha streamed data sample (2 pb^{-1}) has been used to estimate the contamination due to Bhabha events, which is quoted to be at most (0.02 ± 0.01)%.

A similar survey has been performed for the K_μ sample, in which the background has been evaluated as coming from the other charged kaon decays (0.156 ± 0.005)%, from $\phi \not\to K^+K^-$ $(0.03 \pm 0.01)\%$, and from Bhabha's $(0.02 \pm 0.01)\%$.

In summary, the background fractions for the selftags are estimated as

$$\xi^{\theta}_{bckg} = (0.37 \pm 0.02)\% \quad , \quad \xi^{\mu}_{bckg} = (0.21 \pm 0.02)\% \; . \tag{2.15}$$

3 Selection of $K^\pm \to \pi^\pm\pi^0\pi^0$ (τ') events

$K^\pm \to \pi^\pm\pi^0\pi^0$ events are identified searching for a 2-track vertex with a low-momentum daughter track and 4 on-time γ's in the EMC from the two π^0 decays.

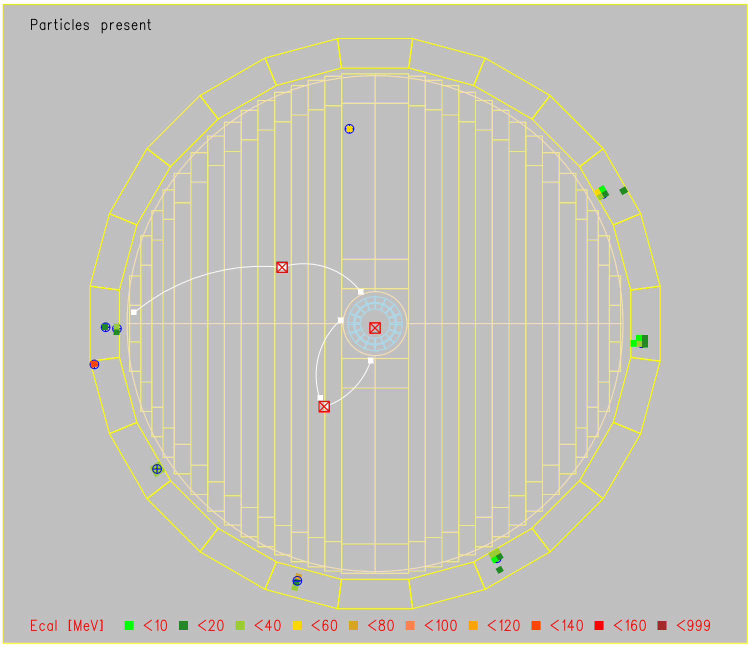

Figure 7: Display of a KLOE event with a $K^+ \to \pi^+\pi^0$ decay (tracks and clusters in the upper part of the picture) and a $K^- \to \pi^-\pi^0\pi^0$ decay (opposite hemisphere).

In Fig. 7 a $\phi \to K^+K^-$ event is shown: the positive kaon (upper left sector of the picture) is a K_θ-selftag, while the K^- decays in the τ' mode in the opposite hemisphere. Six neutral clusters are visible in the EMC (five in the barrel and one in the west-endcap): two of them are associated to the K_θ decay, the other four to the τ' decay.

Ideally, the only physical background should derive from the four-body semileptonic decays: $K^\pm \to l^\pm\pi^0\pi^0\nu_l$ (or $K^{00\pm}_{l4}$), which only differ from the signal in the spectrum of the daughter track momentum.

Actually, the most relevant contributions to background in the τ' come mainly from K_θ and $K^{\pm}_{l3}$ decays in which at least two spurious clusters (*e.g.* splits, accidentals, or unassociated clusters in the tag hemisphere) are found on-time with the two produced by the π^0.

The clusters assigned to photons from the $K^{\mp} \rightarrow \pi^{\mp}\pi^0$ decay in the tagging hemisphere, are excluded from the search of the 4 on-time γ's produced in a τ' decay.

The background contamination in the selected sample will be quantitatively studied in Sect. 4.

3.1 Tracking and vertexing requirements

The selection starts asking, in a self-tagged event, for a vertex made of 2 tracks of the same charge in the DC volume, one of which is a $K^{\pm}$ track. The same requirements listed in Sect. 2.1 for the tag samples are also performed for the τ' decays. The main difference is in the momentum range of the $\pi^{\pm}$ track, which has to satisfy:

$$\bullet) \qquad |\overrightarrow{p}_D| < 135 \ MeV \ . \tag{3.1}$$

in the kaon rest frame. The maximum allowed momentum in the $K^{\pm}$ frame for a charged pion in a $\pi^{\pm}\pi^0\pi^0$ decay is $p_{max} = 132.95 \ MeV$; the value in equation (3.1) has been chosen assuming a $\sim 1\%$ total momentum resolution on the pion track, in such a way to keep a high efficiency for τ' decays (see Sect. 5.1.2) and to reject both the charged kaon 2-body decays and the two semileptonic modes.

3.2 Clustering requirements

Neutral cluster multiplicity is expected to be at least 6 (4) in K_θ- (K_μ-) tagged events containing a detectable τ' decay; due to the clustering algorithm, in a *signal* event the EMC can contain even more clusters that haven't been associated to any track (Fig. 3). As for $K^{\pm} \rightarrow \pi^{\pm}\pi^0$ decays, a minimum cluster energy is required:

$$\bullet) \qquad E_i > 15 \ MeV \ . \tag{3.2}$$

Since all the four photons produced by the two π^0's in a τ' decay originate from the same point (the $K^{\pm}$'s decay vertex), **at least 4 "on-time" neutral clusters** are required in the event. From now on, a cluster is defined as "*neutral*" if it is different from the two ones associated to the charged daughters of both kaons by the track-to-cluster algorithm [24] and, in the K_θ case, from the two already identified as coming from the π^0 belonging to the tag.

The four clusters are "on-time" when their times fulfill the condition

$$\bullet) \quad |\Delta t'_{ij}| < 4 \quad \forall \ i,j = 1,2,3,4 \ (i<j) \ , \tag{3.3}$$

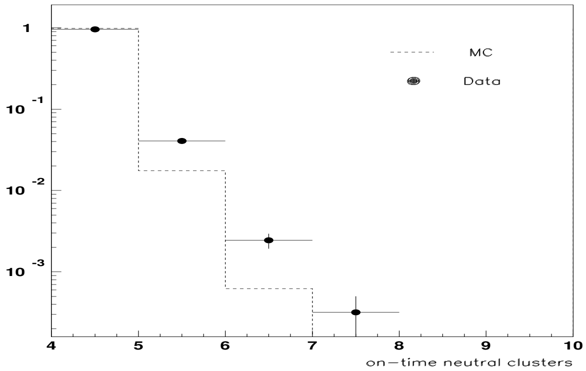

Figure 8: Number of on-time neutral clusters per event for data (dots) and Monte Carlo (solid line).

where $\Delta t'_{ij}$ is defined in equation (2.9).

The number of clusters per event satisfying the cut (3.3) is plotted in Fig. 8 for data and MC. The difference in the shapes of these two distributions does not introduce any bias in the analysis, since the τ' signal is collected asking for *at least* 4 on-time clusters.

A survey on the MC PP0P0 sample has shown that the presence of more than 4 on-time clusters, apart from the rare radiative decay of τ' ($BR < 10^{-5}$), is due to a residual contribution of split and accidental clusters surviving the requirements (3.2) and (3.3). Events with 7 or more on-time neutral clusters are not considered in this analysis since they occur with negligible probability ($\sim 10^{-4}$).

Since the typical energy of charged kaons after the passage through the DC inner walls doesn't exceed $E_K \simeq 505\ MeV$, even if the $\pi^{\pm}$ is produced at very low momentum, the total energy of the other two neutral pions in a τ' decay is not greater than $E_K - m_{\pi^{\pm}} \simeq 365\ MeV$. The relatively poor energy resolution for each single cluster at $80 \div 100\ MeV$ imposes to perform a loose cut, which has been chosen as:

$$\bullet) \qquad E_{tot} \equiv \sum_{i=1}^{4} E_i < 450\ MeV\ , \tag{3.4}$$

where the sum is computed on the 4 most energetic ones,in the case of 5 or more clusters found. In Fig. 9 E_{tot} is plotted for MC and data.

When condition (3.4) is fulfilled, the event is definitively selected and contributes to $N_{tag}^{\tau'}$.

As will be discussed in Sect. 4 the purity reached so far in the final signal sample is satisfactory, but it is worth performing a kinematical analysis on the selected events.

The first step is the "*pairing*" of the four neutral clusters, *i.e.* the correct definition of the two pairs of clusters generated by the two π^0's. As timing information can't help to solve the puzzle, neutral pions are preliminarly reconstructed in the 3 possible hypotheses [6]. Then, a χ^2 function is built for each possible combination of

[6]There are 3 possible pairing hypotheses for reconstructing two π^0's starting from 4 on-time

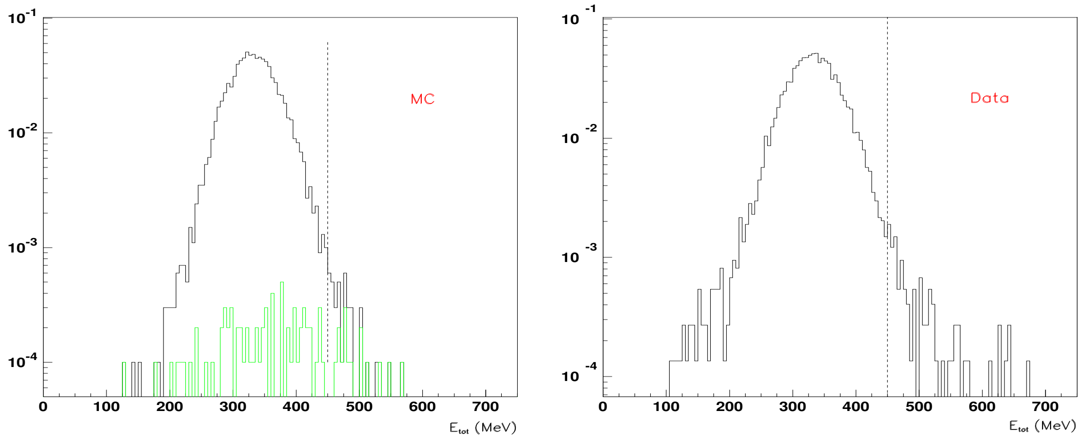

Figure 9: Distributions of the total energy of the clusters selected in the analysis for MC (left) and data (right). In the Monte Carlo plot the dashed superimposed histogram represents the residual background.

clusters pairs, α:

$$\chi^2_\alpha = \left(\frac{E_{\alpha_1\alpha_2} + E_{\alpha_3\alpha_4} + E_D - E_K}{\sigma_E}\right)^2 + \left(\frac{m_{\alpha_1\alpha_2} - m_{\pi^0}}{\sigma_{m_{\gamma\gamma}}}\right)^2 + \left(\frac{m_{\alpha_3\alpha_4} - m_{\pi^0}}{\sigma_{m_{\gamma\gamma}}}\right)^2 \quad (3.5)$$

where $E_{\alpha_i\alpha_j}$ is the energy of each di-photon (α_i, α_j)

$$E_{\alpha_i\alpha_j} = \sqrt{m^2_{\pi^0} + |\overrightarrow{p}_{\alpha_i} + \overrightarrow{p}_{\alpha_j}|^2}$$

and $m_{\alpha_i\alpha_j}$ is the $\gamma\gamma$ invariant mass [7]. In equation (3.5) the standard deviations σ_E and $\sigma_{m_{\gamma\gamma}}$ have been firstly estimated by fitting to a gaussian function the corresponding distributions from Monte Carlo (see Fig. 10).

In the left plots of Fig. 11 the invariant mass $m_{\gamma\gamma}$ computed for the clusters pairs is shown for data and MC, while in the right plots the tri-pion invariant mass ($m_{3\pi}$) distribution is represented. According to Monte Carlo, in both cases the background distribution is flat in the considered mass region. As in the K_θ selection procedure and for the same reasons, both real and simulated data denote a peak at a lower value than the expected π^0 mass in the $m_{\gamma\gamma}$ distribution.

4 Background evaluation in τ' events

Many possible sources of background in τ' decays have been considered, in order to evaluate the purity of the selected τ' sample and to correct $N^{\tau'}_{tag}$ by subtracting the background fraction $\xi^{\tau'}_{bckg}$, in equation (1.7).

clusters. In case of 5 (or 6) clusters found on-time, the number of hypotheses grows to 15 (or 45).

[7]In defining the χ^2 function, no contributions connected to the momentum conservation or to the tri-pion invariant mass have been included, as they don't change by permuting the four photons.

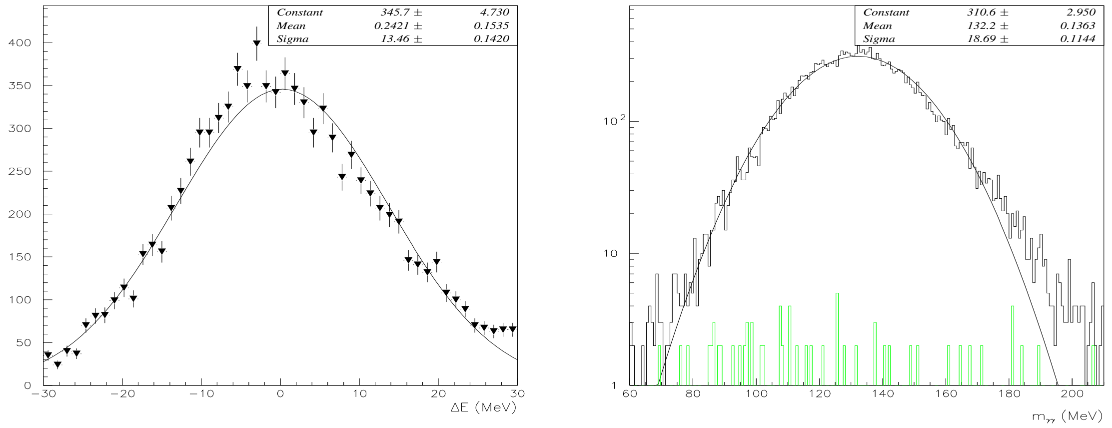

Figure 10: Monte Carlo distributions for energy resolution at the $K^{\pm}$ decay vertex (left) and for $\gamma\gamma$ invariant mass (right) in τ' events; the histogram superimposed on the right represents the wrongly paired clusters.

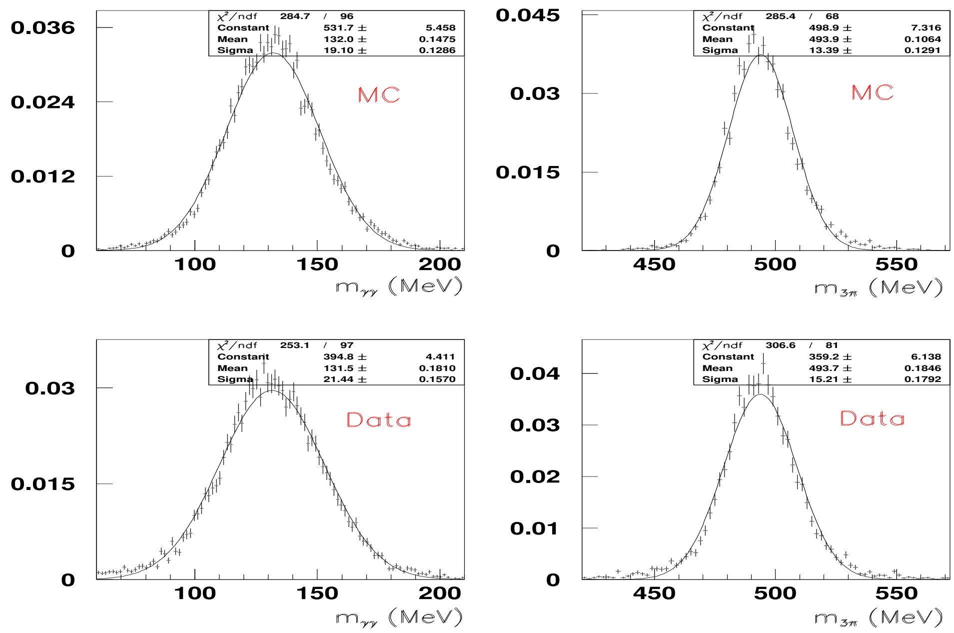

Figure 11: Distributions of clusters pair invariant mass (left) and of tri-pions invariant mass (right), for Monte Carlo (up) and data (down). All the distributions are fitted by gaussian curves.

4.1 Contamination from main $K^{\pm}$ decays

The most copious source of physical background in selecting τ' events comes from the remaining $K^{\pm}$ main decay modes. The contributions from these modes are computed in the ALLPHI Monte Carlo sample and are reported in Tab. 3.

Decay mode	Contamination $\xi^{\tau'}_{bckg}$
$K^\pm \to \mu^\pm \nu_\mu$	$< 0.2 \cdot 10^{-3}$
$K^\pm \to \pi^\pm \pi^0$	$(2.3 \pm 0.4) \cdot 10^{-3}$
$K^\pm \to \pi^\pm \pi^+ \pi^-$	$(0.3 \pm 0.2) \cdot 10^{-3}$
$K^\pm \to e^\pm \pi^0 \nu_e$	$(1.2 \pm 0.3) \cdot 10^{-3}$
$K^\pm \to \mu^\pm \pi^0 \nu_\mu$	$(0.3 \pm 0.2) \cdot 10^{-3}$

Table 3: Contamination coming from the main $K^\pm$ decay modes in the τ' final sample, after the application of the selftags.

The resulting contribution is given by

$$\xi_{main} = (0.41 \pm 0.06)\% \ . \tag{4.1}$$

One additional small contribution to background in K^+K^- events comes from kaons having nuclear interactions with materials of the KLOE apparatus (see Sect. 5.1.1); it has been evaluated from Monte Carlo as:

$$\xi_{nuc} = (0.09 \pm 0.03)\% \ . \tag{4.2}$$

4.2 Contamination from $K^\pm$ rare decays

Charged kaon rare decays, which amount to less than 0.8% of the total decay rate [2], are not simulated in the ALLPHI MC sample; apart from the $K^\pm \to l^\pm \pi^0 \pi^0 \nu_l$ channel, discussed in Sect. 4.3, only few decay modes can exhibit a "τ'-like" topology.

Decay mode	Branching Ratio [2]
$K^\pm \to \pi^\pm \pi^0 \gamma$	$(2.75 \pm 0.15) \cdot 10^{-4}$
$K^\pm \to e^\pm \pi^0 \nu_e \gamma$	$(2.65 \pm 0.20) \cdot 10^{-4}$
$K^\pm \to \mu^\pm \pi^0 \nu_\mu \gamma$	$< 6.1 \cdot 10^{-5}$
$K^\pm \to \pi^\pm \pi^0 \pi^0 \gamma$	$(7.4^{+5.5}_{-2.9}) \cdot 10^{-6}$

Table 4: List of branching ratios [2] of the rare $K^\pm$ decay modes which could enter in the selected τ' sample.

In Tab. 4 the first three listed decay modes have a total probability that doesn't exceed $6.5 \cdot 10^{-4}$, *i.e.* about $3.8 \cdot 10^{-2}$ relative to the τ' signal [8]. They are characterized by a final state including a low-momentum charged particle and 3 photons, so that

[8] This is actually an overestimate, since the total efficiencies for these background sources is expected to be lower than the one for τ'.

they could be selected as τ' decays if a fourth spurious cluster in the EMC is paired with the cluster of the radiated photon. Since the mean probability of finding on-time such two clusters is $P_{w\gamma} \simeq 8\%$ (as described in Sect. 5.2.4), the contamination $\xi_{3\gamma}$ from these channels cannot exceed 0.3%.

For what concerns the $K^{\pm} \to \pi^{\pm}\pi^0\pi^0\gamma$ mode, the corresponding branching ratio is about 2000 times smaller than the parent mode, but all the requirements for the τ' selection are correctly fulfilled. Then the described measurement is inclusive, even though a 0.05% presence of $\tau'\gamma$ decays in the final sample is undetectable at the precision level reached in this analysis.

Other decays as $\pi^0\pi^0\pi^0 e^{\pm}\nu_e$ and $\pi^0\pi^0 e^{\pm}\nu_e\gamma$ are negligible and have been ignored.

4.3 Contamination from $K_{l4}^{00\pm}$ decay

The PDG world fit provides [2, 10, 11]:

$$BR(K_{e4}^{00\pm}) = (2.1 \pm 0.4) \cdot 10^{-5} \ .$$

Up to now there have been no experiments observing $K_{\mu 4}^{00\pm}$ decays, but assuming that the branching ratio for this channel is of the same order of the $K_{e4}^{00\pm}$, one can affirm that the $K_{l4}^{00\pm}$ decay modes occur at least 500 times more rarely than the τ' channel.

The cuts described in Sect. 3 are totally ineffective in rejecting $K_{l4}^{00\pm}$ events because the two π^0's behave exactly in the same way in the background and in the signal. A requirement on the tri-pion invariant mass can't work efficiently if the wrong $\pi^{\pm}$ mass is assigned to the lepton's track in a $K_{l4}^{00\pm}$ vertex.

The MC LP0P0NU sample (10^5 events) have been used to keep as low as possible the contamination due to $K_{l4}^{00\pm}$ decays in the τ' sample. A 3:1 ratio for the $e^{\pm}$:$\mu^{\pm}$ lepton family has been simulated.

About 15% of $K_{l4}^{00\pm}$ events are rejected by the requirement (3.1) on the daughter track momentum using the $\pi^{\pm}$ mass hypothesis ($e^{\pm}$ can reach momenta up to 200 MeV in $K_{l4}^{00\pm}$ decays).

Electrons in the momentum region in which they most likely can be confused with $\pi^{\pm}$'s in τ' decays, are ultrarelativistic ($\beta \sim 1$), while charged pions with $50 \div 150$ MeV momentum have β ranging from 0.3 to 0.7. In order to use this information, the time t_D of the cluster associated to the daughter track is required. In the same time scale, the vertex is created at a time that can be reconstructed from the four clusters γ_j as:

$$t_V = \frac{1}{4}\sum_{j=1}^{4}\left(t_{\gamma_j} - \frac{|\overrightarrow{r}_{V\gamma_j}|}{c}\right) \ , \tag{4.3}$$

so that $t_D - t_V$ gives an estimate of the time of flight (TOF) of the daughter particle. As the length λ_D of the helicoidal trajectory from the vertex to the cluster is measured with good accuracy, the time at vertex can be also extracted from the daughter's TOF as

$$t^{(x)} = t_D - \frac{\lambda_D}{c}\sqrt{1 - \left(\frac{m_x}{p_D}\right)^2} \ . \tag{4.4}$$

where m_x is the daughter mass (m_e, m_μ or m_π).

For the purposes of this analysis, a comparison of the $e^\pm/\pi^\pm$ mass hypothesis can be enough. It is convenient to define the following adimensional quantity:

$$\delta t_{e\pi} = \left(t_V - \frac{t^{(e)} + t^{(\pi)}}{2}\right) \Big/ \left(\frac{t^{(e)} - t^{(\pi)}}{2}\right) \ , \tag{4.5}$$

which is near to 1 if t_V agrees with the electron mass hypothesis, and approaches -1 in case the $\pi^\pm$ mass is appropriate.

Another useful variable is the squared missing mass

$$m_m^2 = (E_K - E_{\pi_1^0} - E_{\pi_2^0} - E_D^{(e)})^2 - |\vec{p}_K - \vec{p}_{\pi_1^0} - \vec{p}_{\pi_2^0} - \vec{p}_D|^2 \tag{4.6}$$

which is expected to peak around 0 for $K_{e4}^{00\pm}$ decays.

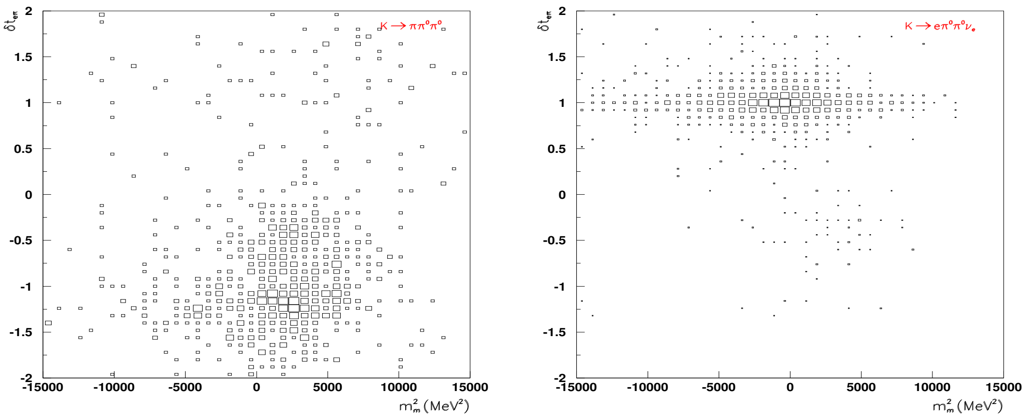

Figure 12: Monte Carlo distributions in the plane of $\delta t_{e\pi}$ vs. m_m^2 (defined in the text) for $K^\pm \to \pi^\pm\pi^0\pi^0$ (left) and for $K^\pm \to e^\pm\pi^0\pi^0\nu_e$ (right). The two distributions are normalized to a different number of events.

In Fig. 12 the bidimensional plots of $\delta t_{e\pi}$ versus m_m^2 are shown for the Monte Carlo samples PP0P0 (left) and LP0P0NU (right). A rectangular cut in this plane could reduce the contamination due to $K_{l4}^{00\pm}$ decays by more than one order of magnitude. On the other hand, the τ' sample would be reduced by $\sim 1\%$, so that the study for an *ad hoc* cut and its specific efficiency should be carried on, introducing additional uncertainties on $N_{tag}^{\tau'}$.

By scaling the PP0P0 and the LP0P0NU samples, the contamination due to the $K_{l4}^{00\pm}$ modes has been evaluated to be:

$$\xi_{kl4} = (0.16 \pm 0.06)\% \ , \tag{4.7}$$

where the error is systematic and comes from the limited knowledge of $BR(K_{\mu4}^{00\pm})$ (it has been varied from 0 to $2 \cdot 10^{-5}$ in the simulation). The estimation (4.7) has been obtained without asking for any selftag, but it is assumed not to depend significantly on the decay in the opposite hemisphere.

4.4 Contamination from non K^+K^- decays

Apart from charged kaon events, other possible processes could simulate the τ' decay topology. The statistically more relevant in the physics of ϕ meson, is represented by $K_L \to \pi^+\pi^-\pi^0$. This decay occurs about 2.5 times more frequently than the τ' decay, *i.e.* :

$$\frac{BR(\phi \to K_S K_L)}{2 \cdot BR(\phi \to K^+K^-)} \cdot \frac{BR(K_L \to \pi^+\pi^-\pi^0)}{BR(K^\pm \to \pi^\pm\pi^0\pi^0)} \simeq 2.5 \ .$$

Events containing this decay are characterized by a 2-track vertex in the DC volume and two low-energy neutral clusters. In order to have a configuration that could emulate a τ' event, the track of one of the two charged pions involved in the vertex should be reconstructed in the wrong direction and then identified as a kaon coming from the IP with suitable momentum; moreover, two spurious clusters should be found on-time with the two produced by the π^0.

Even if a $K_L \to \pi^+\pi^-\pi^0$ decay should satisfy all these very peculiar conditions, the very strict requirements imposed by the tags on the other side of the event would strongly suppress the probability of selecting it as a τ'.

The background in the τ' sample due to non-K^+K^- events has been estimated from the ALLPHI Monte Carlo sample, yielding

$$\xi_{nonK^\pm} < 10^{-5} \ . \tag{4.8}$$

The contamination due to Bhabha events, estimated on a small streamed data sample, has been estimated to be:

$$\xi_{bha} < 10^{-5} \ . \tag{4.9}$$

Machine background events are not simulated in any MC sample (simple addition of spurious hits and clusters is performed on "clean" physical events), then their occurrence in the τ' sample has to be evaluated directly from data. The best known source of background for $\phi \to K^+K^-$ events in DAΦNE is provided by photoproduction events [27], characterized by the so-called "monotracks", which are sometimes not rejected by the event classification algorithms [13]. According to [27], photoproduction should be mainly observed in events with one 2-track vertex [9] having coordinates $r_0 \leq 15\ cm$ and $|z_0| \simeq 40\ cm$ (due to DAΦNE geometrical configuration) and providing evidence for a $\Delta(1232)$ peak in the invariant mass distribution.

Anyway, the use of one-charged-kaon based filter algorithms, the application of the K_θ/K_μ tagging strategies and the requirements on the vertex (2.1) and (2.2)

[9]Events containing one only track are ruled out in the analysis by asking for at least one vertex.

reduce the DAΦNE background at a negligible level. This can be observed in Fig. 13, where no peak (apart from the one nearby the IP) is visible for the z coordinate of the vertex and of the point of closest approach to the beam line, and also the invariant mass at the vertex doesn't show any peak around the Δ resonance.

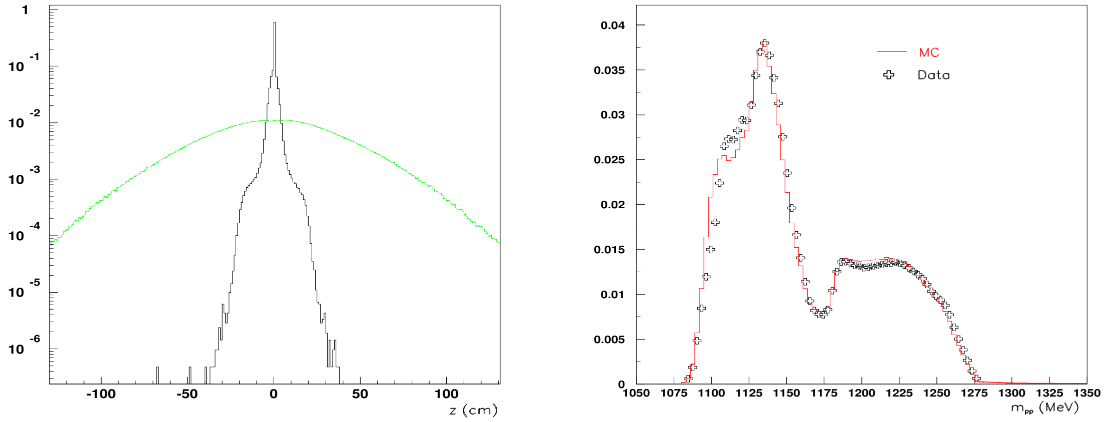

Figure 13: Left: z coordinate of the vertex (green plot) and of the point of closest approach to the beam axis (black plot) for the "kaon" track involved in a K_θ/K_μ selftag. Right: invariant mass when the proton and the charged pion masses are assigned to the two particles in the vertex (crosses are data, solide line is MC); if photoproduction events were still present in the selected sample, a peak should be evident around the $\Delta(1232)$ mass.

4.5 Comparison with data

The total contamination on τ' events coming from the various background sources described so far and simulated in the MC, is:

$$\xi^{\tau'}_{bckg} = \xi_{main} + \xi_{nuc} + \xi_{kl4} + \xi_{nonK^\pm} = (0.66 \pm 0.09)\% \ , \tag{4.10}$$

where all the terms have been supposed independent in obtaining the error.

This estimate of $\xi^{\tau'}_{bckg}$ has to be corrected for the non-simulation of $K^\pm$ rare decays with 3 γ's (Sect. 4.2) and for the possible discrepancies between real data and MC.

Both the finite MC statistics and the relatively small background fraction in the final τ' sample make this correction difficult to be performed. However an estimate of the compatibility of the obtained value with data has been done, as described in the following.

In the MC distribution the ALLPHI sample has been integrated with the corresponding contributions from the LP0P0NU and the data-selected Bhabha samples, proportionally to their relative occurrencies. Given this hypothesis, the distributions of the missing mass m_m (in the hypothesis of $\pi^\pm$ daughter and removing cut (3.1) on p_D) have been studied and compared with data (see Fig. 14). A peak at

Figure 14: Up: Monte Carlo (histogram) and data (crosses) distribution of the missing mass at vertex in the region around the π^0 mass. The shaded histogram below represents the MC contamination.

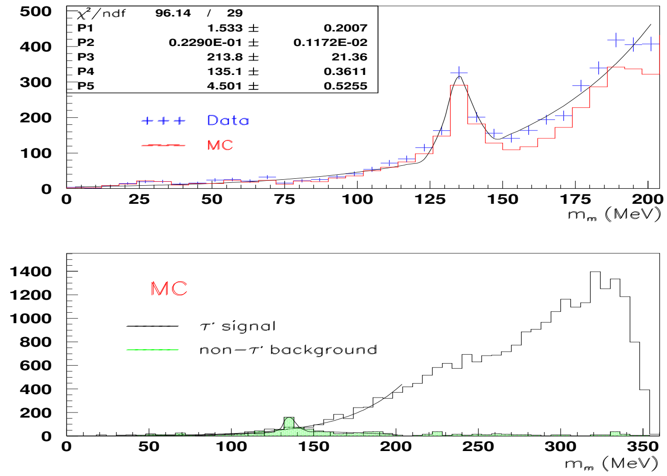

135 MeV due to $K \to \pi\pi^0$ and a smaller remainder background have been fitted on MC to a sum $f_{bckg}(m_m)$ of two gaussians and the curve produced in the distribution by the τ' signal to an exponential $f_{sign}(m_m)$ in the region $[0, 200]$ MeV (the results of the two fits are reported in the figure).

The data distribution has been fitted to $f_{sign}(m_m)+kf_{bckg}(m_m)$, and the resulting parameter $k = 1.13 \pm 0.07$ has been used to correct the MC background estimate:

$$\xi^{\tau'}_{bckg} = (0.75 \pm 0.11)\% \ . \tag{4.11}$$

A similar strategy to correct the MC has been applied to some samples used in the study of the efficiencies (Sect. 5) in order to estimate the background in these samples.

5 Efficiency evaluation

The efficiency $\epsilon^{\tau'}_{sel}$ to select a τ' decay provided that a selftag event has occurred can be factorized as follows:

$$\epsilon^{\tau'}_{sel} \ = \ \epsilon_K \cdot \epsilon_{vtx} \cdot \epsilon_{clu} \cdot \epsilon_{Etot} \ . \tag{5.1}$$

Each single term is related to the cuts described in Sect. 3:

- ϵ_K : efficiency to reconstruct and identify the charged kaon's track in a tagged event, according to the event classification algorithms;
- ϵ_{vtx} : efficiency to reconstruct a 2-track vertex involving the $K^{\pm}$ track and a low momentum daughter track;
- ϵ_{clu} : efficiency to observe and identify four on-time clusters coming from a given vertex, according to the energy and time requirements (3.2) and (3.3);
- ϵ_{Etot} : efficiency to identify a τ' decay process, by applying the cut (3.4) on the total energy of the four clusters.

All the efficiencies listed above could, in principle, be different whether a K_θ or K_μ tag is used: for this reason almost all the studies concerning efficiencies have been repeated for each one of the selftag samples, in order to consider possible differences in the evaluation of $\epsilon_{sel}^{\tau'}$.

In every case, the method to compute these efficiencies makes use of a specific and reliable data *sample of normalization* (**SoN**). The efficiency connected to a *SoN* is evaluated as the fraction of events in the *SoN* that satisfy the corresponding set of requirements applied in the analysis.

Each data *SoN* selection has been studied by using Monte Carlo, from where it's possible to control the purities of the *SoN*s selected. These purities enter in the extraction of the systematic errors for the corresponding efficiency, while the statistical uncertainty on each efficiency comes from the dimensions of the relative *SoN*. Since all of the *SoN*s have been extracted from different data samples of Tab. 2, the obtained results are not statistically correlated.

5.1 Charged track and vertex efficiencies in τ'

In this section the efficiencies ϵ_K and ϵ_{vtx} are discussed.

Since such efficiencies depend on the particular $K^\pm$ decay mode, the method applied to estimate them is to select a *SoN* which emulates as much as possible the τ' sample, but never using drift chamber variables under investigation.

5.1.1 Estimate of ϵ_K

The *SoN* used to evaluate ϵ_K, called `tag+4`, is based on tagged events in which a set of four non-tag clusters fulfills the following kinematical cuts:

- $20\ MeV < E_i < 220\ MeV,\ \forall\ i = 1, \ldots, 4$
- a permutation $(i_k)_{k=1,\ldots,4}$ is such that $135\ MeV < (E_{i_1} + E_{i_2}), (E_{i_3} + E_{i_4}) < 195\ MeV$
- at most 2 clusters with $E_i > 120\ MeV$
- at most 2 clusters with $E_i < 60\ MeV$
- $|t_i - t_j| < 9\ ns,\ \forall\ i, j = 1, \ldots, 4.$

These conditions are justified by the kinematics of the π^0's from the low momentum kaons produced at DAΦNE and are optimized to reject the background from $K \to \pi\pi^0$ and K_{l3}.

The residual contamination arises either from charged kaons going in some non-τ' decay or from nuclear interactions stopping the charged kaons in the chamber materials. Nuclear interactions mainly involve negative kaons, since the resulting total cross section is about 100 mb for K^- and 10 mb for K^+ with momenta below

200 MeV. The Monte Carlo simulation is based on a model [28] which takes into account all the known processes in which a charged kaon can undergo at the typical KLOE energies [10]. An additional requirement is then imposed:

- at least 8 DC hits in the event used by the pattern recognition and not involved in the two tracks of the tag hemisphere.

This reduces, in the `tag+4` sample, the residual contamination that arises from events with high cluster multiplicity in the non-tag hemisphere provoked by nuclear interactions stopping the charged kaon in the materials of the DC walls and of the beam pipe, so producing cascades of neutral particles (mainly neutrons and photons impinging on the EMC) with no DC hits.

To a first approximation, ϵ_K could be measured directly from data as the ratio $N_{tag+4}[K\ found]/N_{tag+4}$, where N_{tag+4} (and $N_{tag+4}[K\ found]$) is the number of events selected in the *SoN* in which the kaon has not interacted (and it has been reconstructed and identified). These numbers still contain the background from non-τ' decays, to be considered in a second step.

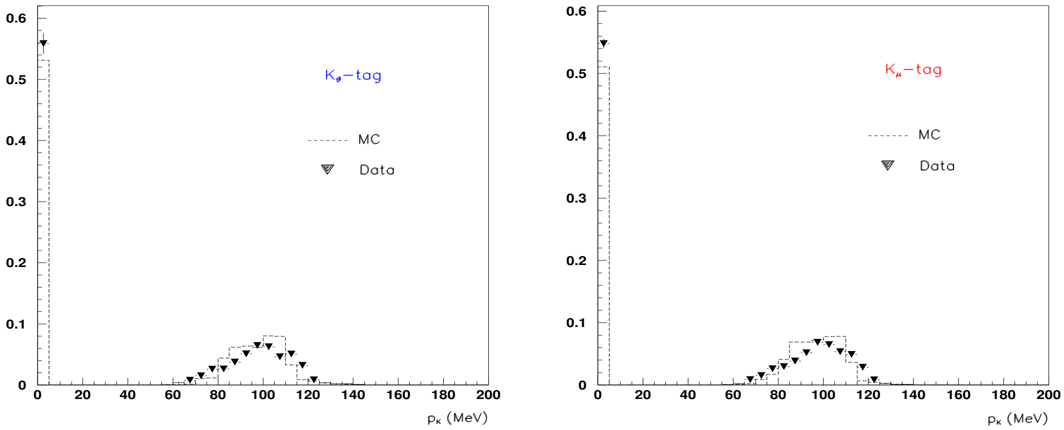

Figure 15: Momentum distributions of the charged kaons found in tag+4 events for data (dotted plot) and for MC (dashed line): left for K_θ-tag and right for K_μ-tag. The single bin at 0 is populated by events in which no kaon track is found.

In Fig. 15 the normalized distribution of the charged kaon momentum is presented for data and Monte Carlo in both the K_θ-`tag+4` and the K_μ-`tag+4` samples; in each plot the first unphysical bin is filled whenever a kaon track is not reconstructed and/or identified.

The ratio ϵ_{obs} that is measured on data is given by

$$\epsilon_{obs} \equiv \frac{N^{obs}_{tag+4}[K\ found]}{N^{obs}_{tag+4}} = \frac{N_{tag+4}[K\ found]}{N_{tag+4}} \cdot \frac{(1+\delta^{N'}_{tag+4})}{(1+\delta^{N}_{tag+4})\cdot(1-\delta^{dec}_{tag+4})}\ , \tag{5.2}$$

[10] One example of reaction occurring to negative kaons stopped in a material is $K^- p \to \Lambda\gamma$, with $\Lambda \to n\pi^0$: the ensemble of neutral clusters produced can happen to satisfy the requirements on the EMC used in the definition of `tag+4`.

where N^{obs}_{tag+4} and $N^{obs}_{tag+4}[K\ found]$ are the numbers of events observed on data, which have to be corrected by means of the following terms:

* δ^{N}_{tag+4} is the contamination fraction in N^{obs}_{tag+4} due to nuclear interactions,
* $\delta^{N'}_{tag+4}$ is the analoguos contamination fraction in $N^{obs}_{tag+4}[found]$,
* δ^{dec}_{tag+4} is the fraction in N^{obs}_{tag+4} of non-interacting kaons, discarded by the cut on the number of DC hits in case the resulting charged particles produce few hits and no tracks in the drift chamber.

The quantities $N_{tag+4}[K\ found]$ and N_{tag+4} have to considered as a sum of a τ' and a non-τ' part.

The second correction to ϵ_K regards the background due to $K^{\pm}$ mesons in `tag+4` that decay in some non-τ' mode: Monte Carlo is used to evaluate the probability of such contamination, P^{bckg}_{tag+4}, subsequently corrected as will be discussed in more detail in Sect. 5.1.2.

Now ϵ_K is defined as the probability for a generic kaon actually decaying in τ' to be identified, and similarly ϵ^{bckg}_K for a kaon decaying in any other channel observed `tag+4`. This leads to the relation

$$N_{tag+4}[K\ found] = \epsilon_K \cdot N^{\tau'}_{tag+4} \ + \ \epsilon^{bckg}_K \cdot N^{bckg}_{tag+4} \ . \tag{5.3}$$

Since the probability for a non-interacting $K^{\pm}$ selected in `tag+4` to decay in τ' is $(1 - P^{bckg}_{tag+4})$, the following relation holds:

$$N^{\tau'}_{tag+4}/N^{bckg}_{tag+4} = (P^{bckg}_{tag+4})^{-1} - 1 \ ,$$

so that ϵ_K can be definitively expressed as

$$\epsilon_K = \left(\epsilon_{obs} \cdot \frac{(1+\delta^{N}_{tag+4}) \cdot (1-\delta^{dec}_{tag+4})}{1+\delta^{N'}_{tag+4}} - P^{bckg}_{tag+4} \cdot \epsilon^{bckg}_K \right) \cdot \frac{1}{1-P^{bckg}_{tag+4}} \ . \tag{5.4}$$

The efficiency ϵ^{bckg}_K has been obtained from data by defining a suitable *SoN* which represents as much as possible the background decays observed in the MC `tag+4` sample, (*i.e.* $K^{\pm} \to \pi^{\pm}\pi^0$, $K^{\pm} \to e^{\pm}\pi^0\nu_e$ and $K^{\pm} \to \mu^{\pm}\pi^0\nu_{\mu}$). This sample, called `tag+2`, is composed by K_{θ} and K_{μ} tagged events in which two (and only two) non-tag neutral clusters have been found to satisfy the requirements:

- $25\ MeV < E_1, E_2 < 225\ MeV$
- $160\ MeV < E_1 + E_2 < 400\ MeV$
- $|t_1 - t_2| < 9\ ns$.

	K^+	K^-
ϵ_{obs}	0.497 ± 0.002	0.495 ± 0.003
δ^N_{tag+4} (MC)	$\sim 10^{-4}$	0.006 ± 0.002
$\delta^{N'}_{tag+4}$ (MC)	$-$	0.004 ± 0.002
δ^{dec}_{tag+4} (MC)	0.059 ± 0.003	0.055 ± 0.003
P^{bckg}_{tag+4} (MC)	0.0198 ± 0.0014	0.0132 ± 0.0015
ϵ^{bckg}_K	0.467 ± 0.001	0.456 ± 0.001
ϵ_K	0.465 ± 0.002	0.467 ± 0.003

Table 5: Summary of the terms involved in ϵ_K for positive and negative kaons.

The lower kinematical cut on the sum of energies reduces the residual presence of τ' in the *SoN*, while the cut on $|t_1 - t_2|$ favors on-time clusters and therefore strongly suppresses $K^\pm \to \mu^\pm \nu_\mu$ and $K^\pm \to \pi^\pm \pi^+ \pi^-$ decays. As a result of the previously listed conditions, the MC `tag+2` sample is essentially made of the three main one-π^0 decays in the percentage of $(98.75 \pm 0.14)\%$, with relative populations in agreement with their known branching ratios. ϵ^{bckg}_K has been estimated on data taking into account $K^\pm$ nuclear interactions and MC-evaluated backgrounds (from 0- and 2-π^0's $K^\pm$ decays) in a similar way as done in (5.2).

All the quantities defined so far have been measured both on data (sample A) and on MC; they are summarized in Tab. 5 separately for K^+ and K^-, to control different effects ascribed to nuclear interactions, but in this analysis only the total average values have been considered for each one of them.

The efficiency ϵ_K is then obtained from (5.4):

$$\epsilon_K = 0.466 \pm 0.001_{stat} \pm 0.002_{syst} \ . \tag{5.5}$$

The systematic error includes the contributions of the various terms obtained from MC. The uncertainties on δ^N_{tag+4} and $\delta^{N'}_{tag+4}$ are dominated by the limited knowledge on the $K^\pm$ cross section describing the nuclear interactions and on the precision to which the thickness of the materials used are described in the MC. The MC estimates of δ^{dec}_{tag+4} and P^{bckg}_{tag+4} include as an error the difference between the two types of tag applied to `tag+4`.

It should be noticed that ϵ_K includes the contribution of the geometrical acceptance, due to kaons that decay before reaching the detector and/or interact with the materials of the apparatus.

5.1.2 Estimate of ϵ_{vtx}

The efficiency to find a 2-track vertex with a $K^\pm$, in general, depends on the kaon decay since the daughter track can have different momentum spectra. The total vertex efficiency ϵ_{vtx} can be parametrized as:

$$\epsilon_{vtx} = \epsilon_v \cdot \epsilon_{t2v} \cdot \epsilon_{pdau} \ , \tag{5.6}$$

where ϵ_v is the efficiency to find a 2-track decay vertex including the already found kaon track, and ϵ_{pdau} and ϵ_{vtx} are, respectively, the efficiencies of the cut on the tracks-to-vertex distance (2.2) and of the daughter momentum requirement (3.1), once the vertex has been already found.

Two data samples are used in this analysis for the evaluation of ϵ_{vtx}: the first one (`tag+4+K`) concerns ϵ_v, while the other one (`tag+4+v`) is used to study ϵ_{t2v} and ϵ_{pdau}.

The `tag+4+K` is the `tag+4` sample in which a kaon track has been identified in the non-tag hemisphere (with a charge opposite to the kaon tag). The purity of this *SoN* is higher than in `tag+4` (0.989 ± 0.001).

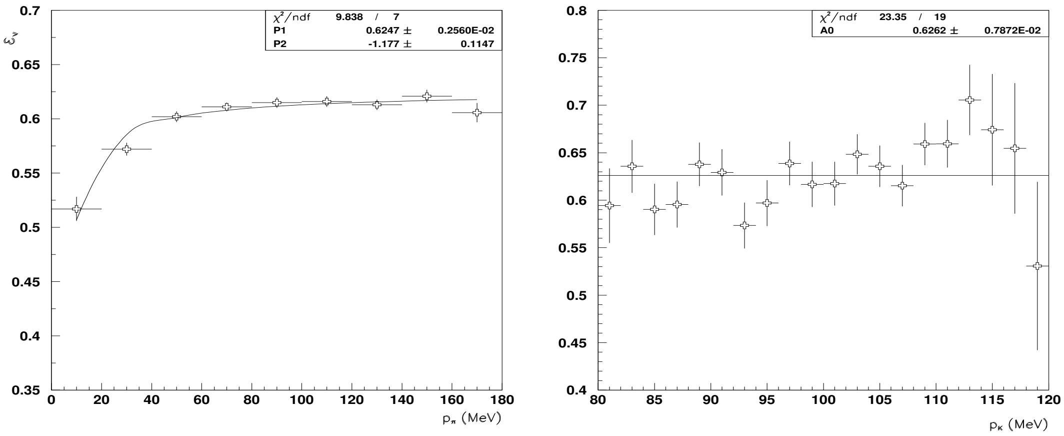

Figure 16: Efficiency ϵ_v (K_θ-tag is applied). Left: as a function of the daughter momentum. Right: as a function of the momentum of the $K^\pm$ track. Both momenta are the ones measured in the laboratory frame.

In Fig. 16 the efficiency ϵ_v is represented as a function of the expected momentum of the daughter track p (left) and of the kaon track (right). The first quantity is evaluated from the energies of the kaon and of the four clusters:

$$p^* = \sqrt{\left(E_K - \sum_i E_i\right)^2 - m_{\pi^\pm}^2} \ . \tag{5.7}$$

The difference between p^* and the momentum given by MC at vertex is normally distributed around 0 with $\sigma \simeq 4\ MeV$, then the choice of a 20 MeV binning in the plot is justified.

The shape of $\epsilon_v(p)$ shows that the probability to reconstruct a vertex decreases as soon as the outcoming track has momentum lower than $\sim 50\ MeV$. This effect is important for daughter tracks in τ' decays, which can get quite low momenta in the

Figure 17: Momentum distribution in the laboratory frame of the tracks selected as pions in τ' events, for data (dots) and Monte Carlo (solid line).

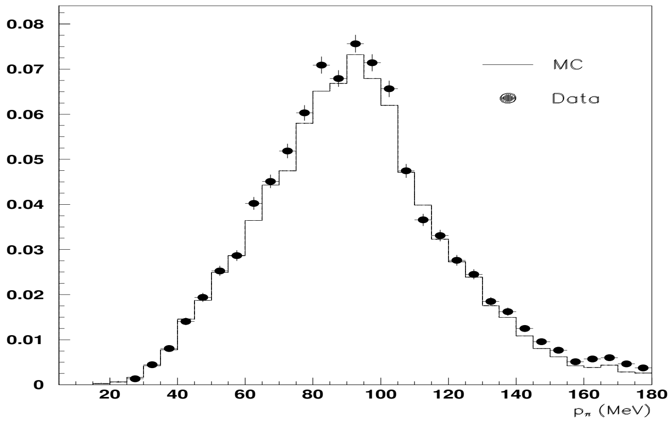

laboratory frame (see Fig. 17). A simple parametrization of ϵ_v versus the daughter momentum p is:

$$\tilde{\epsilon}_v(p) = a - b/p \ ,$$

and can be used to fit the left plot in Fig. 16. The results obtained ($a = 0.625 \pm 0.003$ and $b = 0.118 \pm 0.11\ MeV$) allow to estimate the vertex efficiency ϵ_v, as an average over the momentum distribution $\varphi(p)$:

$$\epsilon_v = \frac{\int \tilde{\epsilon}_v(p)\varphi(p)dp}{\int \varphi(p)dp} \ . \tag{5.8}$$

In the resulting value, obtained from the data sample B,

$$\epsilon_v = 0.601 \pm 0.002_{stat} \pm 0.002_{syst} \ ,$$

the systematic error takes into account the difference in ϵ_v coming from the two different tags.

A compatible result for ϵ_v ($0.5997 \pm 0.0010_{stat}$) can be obtained as the relative ratio of decays in the `tag+4+K` sample, in which at least a 2-track vertex in the DC volume (*i.e.* with $r > 25\ cm$) involving the kaon track has been found (regardless of the daughter track momentum).

The flatness of the right plot in Fig. 16 is taken here as a proof of the independence of ϵ_v from the momentum of the decaying kaon.

The information about the vertex connected to the $K^\pm$ track in `tag+4+K` defines a new *SoN*: `tag+4+v`. From this sample both the efficiencies ϵ_{t2v} and ϵ_{pdau} have been evaluated. The cuts (2.2) and (3.1) concerning these two efficiencies have been requested since the first one improves the quality of the vertex and the second one is based on kinematics. Therefore, ϵ_{t2v} and ϵ_{pdau} have been assumed to be uncorrelated and independent, have been estimated on separate data samples (C and D, respectively), and any residual correlation has been considered as a source of systematics.

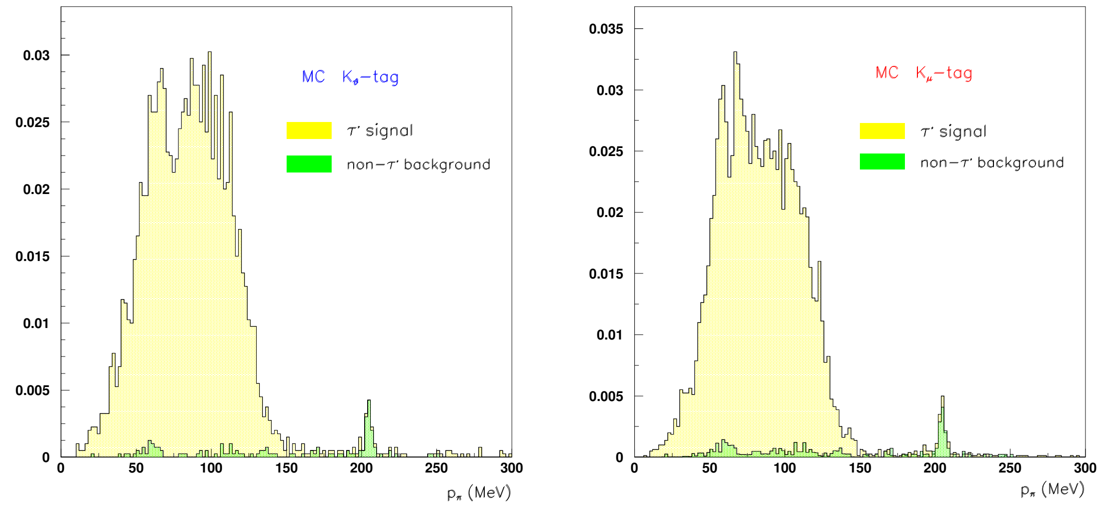

Figure 18: Momentum distributions in the $K^{\pm}$ rest frame for the daughter tracks in the tag+4+v MC samples when K_{θ}-tag (left) and K_{μ}-tag (right) is applied. The shaded areas represent the contamination due to non-τ' decays.

The background in the `tag+4+v` MC sample is shown in the shaded histograms in Fig. 18 for K_{θ} and K_{μ} tagged events as functions of the daughter track momentum in $K^{\pm}$ frame: for both tags the contamination is quite uniform in the range allowed for the τ' decay, while a peak appears around 205 MeV, due to residual $K \to \pi\pi^0$ vertices. The shape of contamination on data is assumed to be as observed on MC, amplified by a factor calculated from the ratio of the normalized [11] integrals under the $K \to \pi\pi^0$ peaks between data and MC. In Fig. 19 the distribution of

Figure 19: Distribution of the daughter momentum in the kaon rest frame for data before (line) and after (dots) background subtraction.

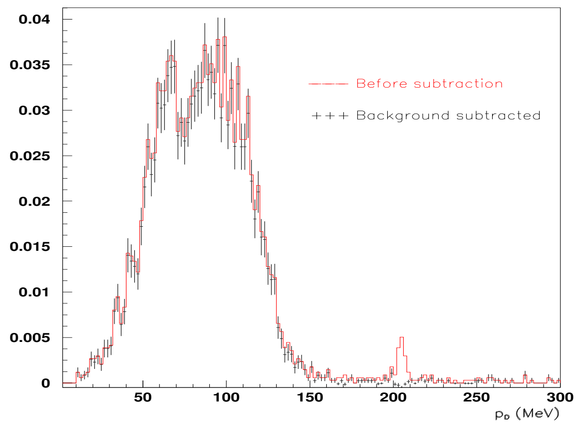

the daughter momentum in $K^{\pm}$ frame is shown before (solide line) and after (dots) background subtraction.

The efficiency ϵ_{t2v} has been computed as the fraction of vertices in `tag+4+v`

[11] The normalization is done on the integrals over the interval $[0, 135]$ MeV, where the τ' purity is maximized.

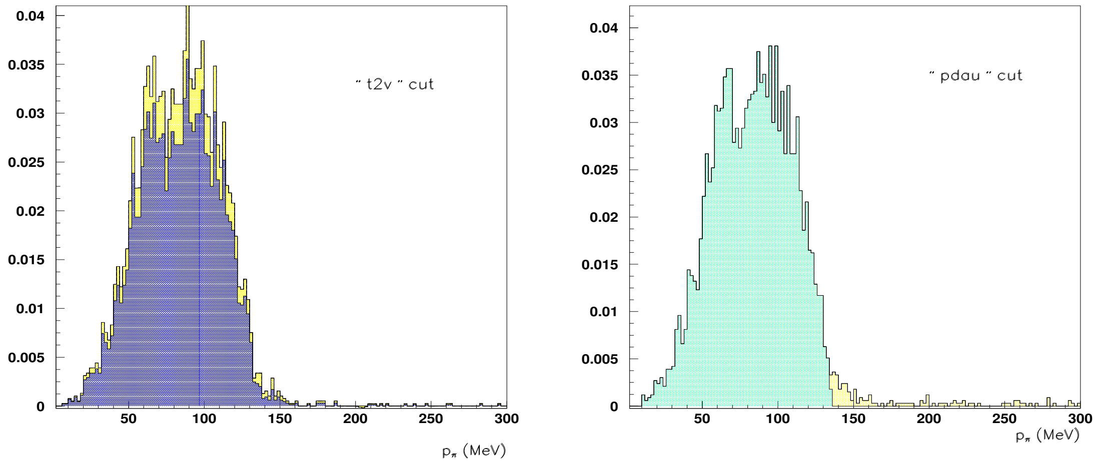

Figure 20: Normalized momentum distribution in the $K^{\pm}$ rest frame for the daughter tracks in tag+4+v for background-subtracted data. In the left plot the coloured area represents the efficiency of the tracks-to-vertex cut (2.2). In the right plot the coloured area defines the efficiency of the $p_D < 135\ MeV$ requirement.

satisfying the requirement $max\{d(K^{\pm}_{LH}, V), d(\pi^{\pm}_{FH}, V)\} < 50\ cm$ (left plot of Fig. 20). As for ϵ_{pdau}, this efficiency is calculated as the integral between 0 and 135 MeV of the momentum distribution (right plot of Fig. 20). They are reported in Tab. 6 for data and MC.

Systematic errors have been evaluated by studying possible correlations between ϵ_{t2v} and ϵ_{pdau} and from the background subtraction (the purity of `tag+4+v` is about 0.995 with both the two tags).

Finally, ϵ_{t2v} and ϵ_{pdau} have been checked separately on both the `tag+4+v` samples defined by the K_{θ}- and the K_{μ}- tag, and found independent of the tag adopted.

Tab. 6 contains a summary of all the efficiencies involved in ϵ_{vtx}, with errors including both statistical and systematic contributions.

Efficiency	Data	MC
ϵ_v	0.601 ± 0.003	0.607 ± 0.006
ϵ_{t2v}	0.922 ± 0.002	0.924 ± 0.004
ϵ_{pdau}	0.972 ± 0.002	0.978 ± 0.003
ϵ_{vtx}	0.539 ± 0.003	0.548 ± 0.006

Table 6: Summary of the efficiencies factorized in ϵ_{vtx}.

When in a given event both K^+ and K^- tracks have been identified, it is sometimes possible to reconstruct a ϕ vertex nearby the interaction point (IP), but a wrong extrapolation toward the IP may happen and even more than one ϕ vertex can be found in a $\phi \to K^+K^-$ event. It should be remarked that, because of faults in the procedures of vertex/track reconstruction, more than one vertex in the DC volume (apart from ϕ vertices) could be found to include the kaon. However, the possibility to ask for only one of these non-ϕ vertices has been exploited without any appreciable gain in purity of the selected τ' sample.

5.2 Cluster efficiencies in τ'

The efficiency ϵ_{clu} to find four clusters in the τ' decay has been factorized as a product of two terms:

$$\epsilon_{clu} = \langle A^4_{clu} \rangle \cdot \epsilon_{4onT} \ , \tag{5.9}$$

where A_{clu} represents the single cluster acceptance for each of the four τ' final state photons and ϵ_{4onT} is the efficiency of the cuts (3.2) and (3.3).

5.2.1 Estimate of A_{clu}

A_{clu} has been parametrized as a function of the cluster energy E_γ and has been estimated for photons produced in $K^\pm \to \pi^\pm\pi^0$ decays, in which the photon energy spectrum has been weighted to reproduce the one from τ'. From a geometrical point of view, photons from $K^\pm \to \pi^\pm\pi^0$ and $K^\pm \to \pi^\pm\pi^0\pi^0$ are produced with the same spatial distribution at the $K^\pm$ decay vertex, and propagate with a uniform angular distribution before impacting on the calorimeter.

The *SoN* used for the evaluation of A_{clu}, `Kp+1`, is selected from data and MC according to the drift chamber requirements for the K_θ sample described in sections 2.1 and 2.2.1. The cluster associated to the pion daughter track is required in accordance with the track-to-cluster algorithm. Let d_π be the length of the flight path of the charged pion and β_π its velocity: a neutral cluster (γ_1 in Fig. 21) with energy E_1 and distance d_1 from the vertex is requested in the event, such that the time difference $\Delta t_{\pi 1}$ satisfies:

$$\frac{|\Delta t_{\pi 1} - (d_1 + d_\pi/\beta_\pi)/c|}{\sqrt{\sigma_t(E_1)^2 + \sigma_t(E_\pi)^2}} < 3 \ ,$$

and

$$\frac{|E_1 - \tilde{E}_1|}{\tilde{E}_1} < \frac{5\%}{\sqrt{\tilde{E}_1(GeV)}} \ ,$$

where "$\tilde{E}_1$" is the true energy of the neutral cluster estimated from the knowledge of the versor along the vertex-cluster direction, $\overrightarrow{c}_1$:

$$\tilde{E}_1 = \frac{m^2_{\pi^0}}{2\left[(E_K - E_\pi) - (\overrightarrow{p}_K - \overrightarrow{p}_\pi)\cdot\overrightarrow{c}_1\right]} \ .$$

The purity of `Kp+1` can be defined as the percentage of events in which the selected neutral cluster actually comes from a photon of a $K^\pm \to \pi^\pm\pi^0$ decay, and is estimated from MC to be as high as 0.9956 ± 0.0006.

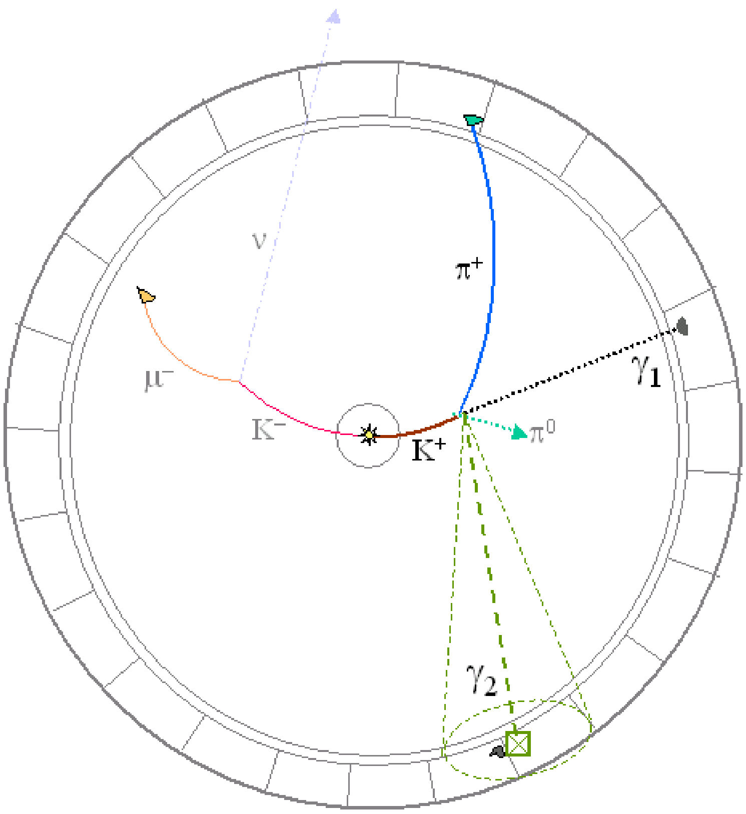

Figure 21: Typical $K^+ \rightarrow \pi^+\pi^0$ event selected in the Kp+1 sample.

By closing the kinematics at the vertex, the four-momentum $(E_{\gamma_2}, \overrightarrow{p}_{\gamma_2})$ of the other photon (γ_2 in Fig. 21) and its flight direction and the expected impact point P_2 on the EMC can be calculated.

Figure 22: Resolution for E_γ in MC Kp+1 sample.

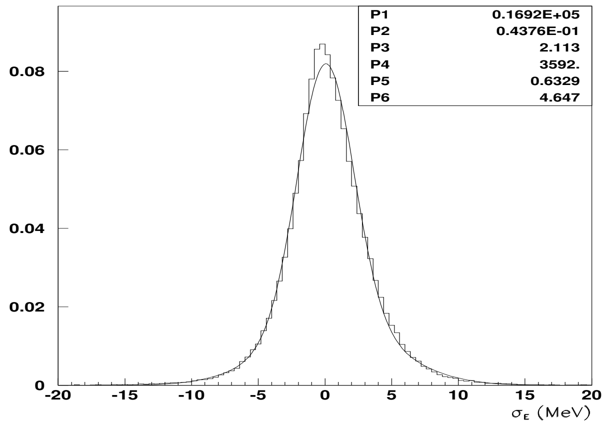

The accuracy in the determination of E_γ ($\equiv E_{\gamma_2}$) has been studied in the Monte Carlo `Kp+1` sample. The distribution is fitted with two gaussians (see fit in Fig. 22). Then, for each E_γ bin, the cluster acceptance A_{clu} is evaluated as the probability to find in a `Kp+1` event a cluster j within spherical space region of radius Δ_c from P_2

[12] that satisfies extremely loose time and energy cuts, according to what expected for γ_2 [13].

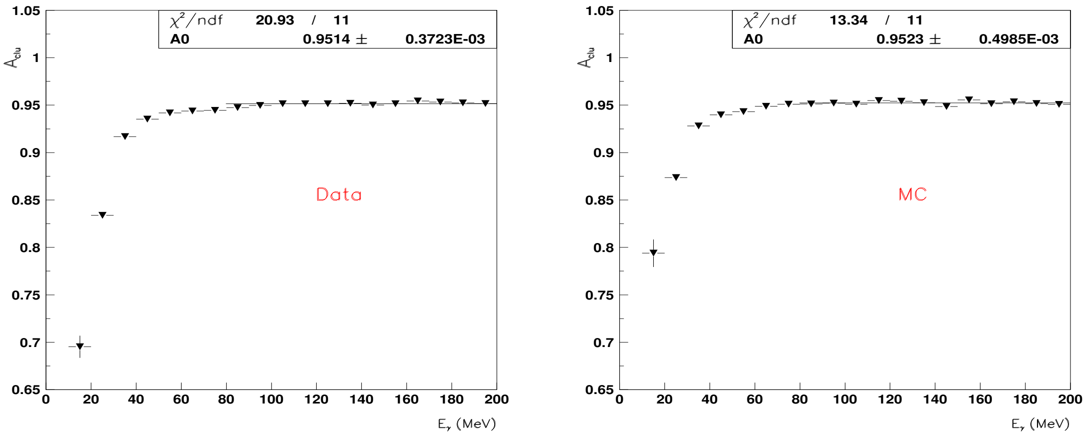

Figure 23: Cluster acceptance for photons in $K \to \pi\pi^0$ events as a function of their expected energy E_γ computed for $\Delta_c = 100$: the plot on the left refers to data, while the one on the right is obtained from MC. In both cases the plateau has been fitted to a constant value.

In Fig. 23 the plot of $A_{clu}(E_\gamma)$ is shown for data (left) and for MC (right) when Δ_c is fixed to 100 cm. As the curves reach the plateau (at $\sim 80\ MeV$), the acceptance becomes purely geometrical. Since the Monte Carlo sample ALLPHI correctly reproduces the data, it has been used to compute the systematics on A_{clu} to be applied on the data-extracted curve.

The acceptance A_{clu} has to be corrected by a factor $\zeta(\Delta_c)$, obtained from Monte Carlo, which takes into account the cases in which a spurious cluster enters in the acceptance region instead of γ_2 or γ_2 is found not where expected, etc. The quantity $\zeta(\Delta_c)$ slightly depends on the choice of Δ_c, as can be seen in Tab. 7; it is shown in the left panel of Fig. 24, including the systematic error coming from the choice of Δ_c [14].

Then the corrected acceptance

$$A_{clu} = \frac{N_{Kp+1}(\Delta_c)}{N_{Kp+1}} \cdot \zeta(\Delta_c) \tag{5.10}$$

[12] It has been preferred to define a spherical space region of given radius Δ_c around P_2 rather than setting an acceptance cone of a fixed semiaperture, since the area that it would intercept would depend on the cylindrical geometry of the EMC and mainly on the position of the vertex, whereas the resolution on the cluster position is approximately constant in the barrel as in the endcaps.

[13] By asking for $\Delta t'(\gamma_1, \gamma_j) < 10$ and for $|E_j - E_2|/E_2 < 10 \cdot 5\%/\sqrt{E_2(GeV)}$, the fraction of background clusters observed nearby the expected position P_2 is strongly reduced, without losing signal.

[14] Δ_c has been moved around 100 cm by ± 20 cm, which is the typical minimum distance between two distinct clusters in the EMC.

	$\Delta_c = 80\ cm$	$\Delta_c = 100\ cm$	$\Delta_c = 120\ cm$
$\zeta(\Delta_c)$	1.0056 ± 0.0012	1.0045 ± 0.0011	1.0042 ± 0.0011

Table 7: Dependence of $\zeta(\Delta_c)$ from Δ_c. The values are averaged over E_γ.

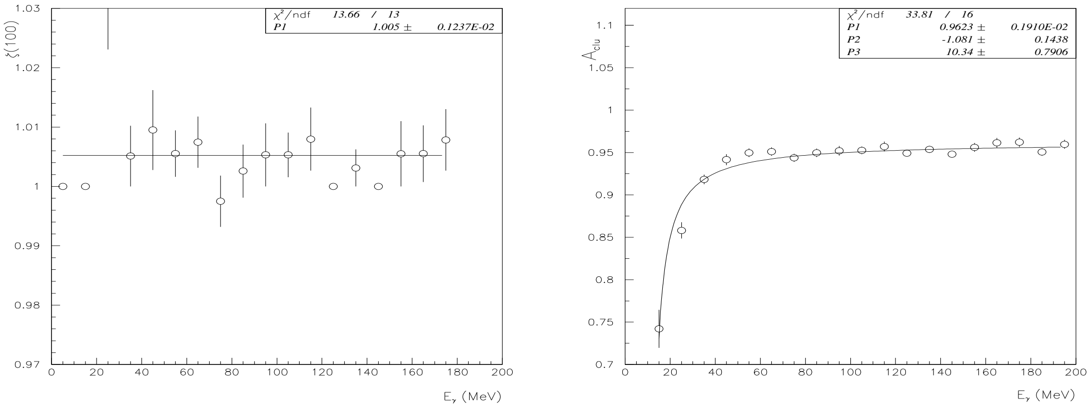

Figure 24: Left: corrective multiplicative factor $\zeta(\Delta_c)$ for A_{clu}. Right: Cluster acceptance $A_{clu}(E_\gamma)$ after the corrections discussed in the text; the fit refers to the function (5.11), with P_1 adimensional parameter and P_2, P_3 expressed in MeV.

is computed and reported in right panel of Fig. 24.

Finally, A_{clu} has been parametrized according to the function:

$$A_{clu}(E) = P_1 - \frac{P_2}{E - P_3} \ , \tag{5.11}$$

with the results of the fit reported in Fig. 24, and $\langle A^4_{clu} \rangle$ on the final sample of τ' decays has been obtained from data as:

$$\langle A^4_{clu} \rangle = \frac{1}{N^{\tau'}} \sum_{i=1}^{N^{\tau'}} \left(\prod_{j=1}^{4} A_{clu}(E_j) \right) \ . \tag{5.12}$$

It turns out that:

$$\langle A^4_{clu} \rangle = 0.799 \pm 0.001_{stat} \pm 0.003_{syst} \ ,$$

where the systematic error derives from the uncertainties of the parameters in the fit of $A_{clu}(E)$.

5.2.2 Cluster time resolutions

The sample `Kp+1` has been used in order to estimate the time resolution $\sigma_t(E)$ for clusters from $K^{\pm}$'s decay vertices. In particular the used subsample is defined as a `Kp+1` decay for which the γ_2 cluster has been successfully found.

When the pair of clusters (γ_1, γ_2) is found, the quantity Δt_{12}, defined according to (2.8), is expected to be normally distributed with standard deviation

$$\sigma(\Delta t_{12}) = \sqrt{\sigma_t(E_1)^2 + \sigma_t(E_2)^2}\ ; \tag{5.13}$$

supposing that $\sigma_t(E) \sim E^{-1/2}$ without systematic terms, (5.13) can be rewritten as

$$\sigma(\Delta t_{12}) = \sigma_t(E_1) \cdot \sqrt{1 + E_1/E_2}\ , \tag{5.14}$$

then the time resolution as a function of energy E_1, $\sigma_t(E_1)$, can be extracted as the standard deviation of the gaussian fit of $\Delta t_{12}/\sqrt{1 + E_1/E_2}$.

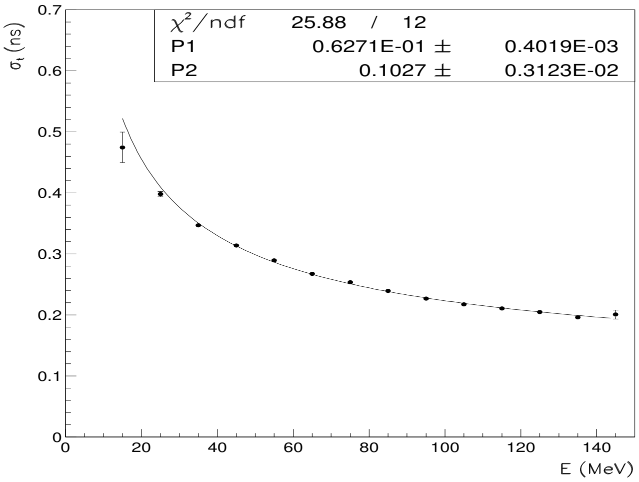

Figure 25: Time resolution (in ns) for clusters associated to neutral pions in $K^{\pm} \to \pi^{\pm}\pi^0$ decays, as a function of their energy (in MeV).

Then, $\sigma_t(E_1)$, extracted from `Kp+1` data and plotted in Fig. 25, provides for the time resolution:

$$\sigma_t(E) \simeq 61\ ps/\sqrt{E(GeV)} \oplus 120\ ps\ , \tag{5.15}$$

differently from MC, which confirms the relation (2.5) The value (5.15) has been used for the real data samples through all the analysis.

5.2.3 Estimate of ϵ_{4onT}

The efficiency to find on-time the four accepted clusters produced in a τ' decay, ϵ_{4onT}, cannot be easily factorized as a product of more elementary probabilities.

A suitable *SoN*, `K+d`, has been used firstly requiring the drift chamber preselection (Sect. 3) in tagged events. Then, a set of clusters in the event is selected, coherently with what done in the analysis, having energy greater than 15 MeV and not involved in the tag hemisphere, nor associated to any of the kaon daughter tracks. A very loose cut is subsequently applied on the times of the clusters left: once defined d_m (d_M) as the minimum (maximum) distance between the vertex and the EMC surface, the quantity

$$\delta\bar{t} = \frac{d_M - d_m + 2\rho_V^{max}}{c} \oplus 2\delta t_c^{max}$$

is defined, where ρ_V^{max} and δt_c^{max} are, respectively, the typical maximum distance reconstructed-true vertex position and the maximum time spread for a generic EMC cluster. The values chosen from the MC ($\rho_V^{max} = 100\ cm$ and $\delta t_c^{max} = 1\ ns$) ensure that 100% of the τ' quartets of clusters have absolute times which are contained within a $\delta\bar{t}$ time window.

A $K^{\pm}$ decay vertex is finally selected as `K+d` if at least one of the quartets extracted from the possible multiplets of clusters found in the event satisfies the additional conditions:

- $20\ MeV < E_i < 220\ MeV$, $\forall\ i = 1, \ldots, 4$
- a permutation $(i_k)_{k=1,\ldots,4}$ is such that $135\ MeV < (E_{i_1} + E_{i_2}), (E_{i_3} + E_{i_4}) < 195\ MeV$
- at most 2 clusters with $E_i > 115\ MeV$
- at most 2 clusters with $E_i < 60\ MeV$.

Apart the very safe request on times, only information on the cluster energies has been used for the selection; no other variables like di-photon invariant masses, four-momentum conservation at vertex, etc., have been considered here, in order not to convolve possible effect due to tracking and vertexing in the selected sample.

The efficiency ϵ_{4onT} is then computed as the fraction of events in `K+d` that get through the requirements (3.2) and (3.3).

The background contamination $\xi_{K+d} = 0.035 \pm 0.004$ given by Monte Carlo is corrected looking to data by comparing the peaks in the missing mass at the vertex (as done for the cut (3.4) in Sect. 5.2.5); in the MC ALLPHI sample $\sim 3\%$ of the non-τ' vertices selected in `K+d` satisfy the on-time condition (3.3) required in the analysis.

From the results reported in Tab. 8 for both K_θ- and K_μ- tagged `K+d` samples (the data sample B has been used), it is evident that the MC is not able to reproduce data and that ϵ_{4onT} has to be separately calculated for the two tags, providing two different estimations for the branching ratio (1.7) to be suitably weighted for the final result [15].

The statistical and systematic errors on the estimations of ϵ_{4onT} come from the *SoN* statistics collected in the *SoN*, and from the uncertainty of background subtraction, respectively.

5.2.4 Spurious clusters in K^+K^- events

The probability $P_{w\gamma}$ for a "spurious" neutral cluster to be found on-time with the γ's from a π^0 decay is studied from a data sample of $K_\theta^+\ K_\theta^-$ events. In these events

[15] The disgreement between data and Monte Carlo in the result of ϵ_{4onT} has been accurately studied in order to understand the main effect responsible of it. The most reliable interpretation of this study is that timing and/or clusters identification are not perfectly simulated in MC.

	Data	MC
$\epsilon_{4onT,\theta}$	0.697 ± 0.004	0.824 ± 0.006
$\epsilon_{4onT,\mu}$	0.745 ± 0.004	0.876 ± 0.005

Table 8: Comparison between data and MC on efficiency ϵ_{4onT} for K_θ- and K_μ-tagged K+d samples.

the association of the two cluster pairs to the respective π^0's is estimated from MC to be the correct one in the $\sim 99.5\%$ of the times.

Given a K_θ vertex and the clusters/photons produced by its π^0, $P_{w\gamma}$ is then evaluated as the probability for any other generic cluster i in the event to satisfy the on-time cut ($|\Delta t'_{ij}| < 4$, $j = 1, 2$), as applied in the analysis for τ' decays.

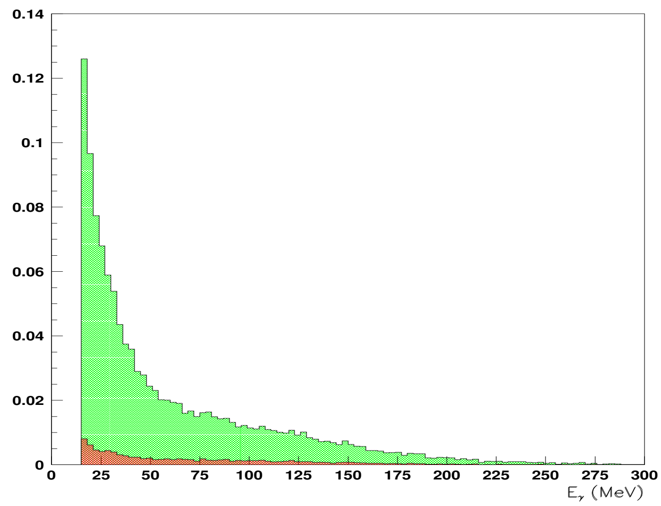

Figure 26: Energy distributions of neutral clusters: green histogram represents all neutral clusters, red histogram indicates the fraction of those which are wrongly found on-time with a *correct* pair of π^0's clusters.

The energy distribution for these clusters after the requirement $E > 15\ MeV$ is plotted in Fig. 26 and compared with the energy spectrum of all the neutral clusters: the ratio between the two integrals yields the average estimate

$$P_{w\gamma} = 0.0786 \pm 0.0014\ , \tag{5.16}$$

which is assumed to be valid also in K_μ tagged events.

5.2.5 Estimate of ϵ_{Etot}

The efficiency to select a τ' according to the cut (3.4) on the total energy of the neutral clusters given by MC is:

$$\epsilon_{Etot}(MC) \ = \ 0.9970 \pm 0.0006_{stat} \pm 0.0007_{syst}\ . \tag{5.17}$$

After the correction taking into account the larger contamination in the data, estimated from the distribution of the missing mass at vertex (see Sect. 4.5), the efficiency becomes:

$$\epsilon_{Etot} \;=\; 0.9947 \pm 0.0006_{stat} \pm 0.0012_{syst} \;, \tag{5.18}$$

where the error is dominated by the finite statistics of the MC sample and by the systematics coming from the difference between K_θ- and K_μ- tags.

6 Systematics and residual effects

Effects not previously discussed coming from the tag, the criteria adopted in the analysis and, finally, the cosmic veto and the FILFO algorithm are investigated.

6.1 Systematics on clustering

The efficiency ϵ_{tag} to reconstruct a K_θ- or K_μ- selftag cancels out in the ratio $N^{\tau'}_{tag}/N_{tag}$ in (1.7), in the hypothesis that the tag is completely uncorrelated by the rest of the event and the selftriggering condition is determined exactly by the only clusters produced in a K_θ/K_μ decay.

More generally, it would be enough that the entity of the eventual correlations between the tag and the non-tag hemispheres had the same effect for the τ' mode and for (the average of) the others in order not to bias the final measurement of the branching ratio.

In practice, there are some peculiar features that make the τ' decay mode subject to a higher probability of "interference" with a K_θ-selftag than other decay modes. This implies, for example, that $\epsilon_\theta/\epsilon^{\tau'}_\theta$ is not exactly 1. The clustering plays a fundamental role in this game, since in no other relevant $K^\pm$ decay channels such a high cluster multiplicity is expected. The Monte Carlo sample PP0P0 has shown that with very low probability ($\sim 10^{-4}$) a cluster (neutral or not) coming from a τ' decay is found so near to another (belonging to a K_θ decay in the opposite hemisphere) that they are reconstructed as one single instead of two [16].

Other possible sources of systematics that have been analyzed regard the criteria applied to select τ':

a) definition of *neutral* clusters,

b) lower cut on the cluster energy ($E_i > 15\ MeV$),

c) on-time requirement ($\Delta t'_{jk} < 4$),

d) the splitting recovery algorithm.

In tagged events, a minimal requirement for a cluster to be *neutral* in a τ' decay is to be:

[16] When two particles separately produce two clusters in the EMC within a rather small distance (less than 20 cm) and with similar times, they can happen to be merged in one single cluster. This rare effect acts as a sort of unacceptance even for well-reconstructed clusters; it has been implicitly considered in Sect. 5.2 when evaluating A_{clu}.

a_0) different from the cluster connected to the $\pi^\pm$ track of τ'.

Apart from this requirement, in general, other conditions can be considered to define a *neutral* cluster:

a_1) not associated to the daughter track in the tag hemisphere,

a_2) not associated to γ's from the tag hemisphere (only if K_θ),

a_3) not associated to any charged track in the event ($a_3 \Rightarrow a_1$, $a_3 \Rightarrow a_0$).

In the present analysis the condition $a_0 + a_1 + a_2$ is used, but other configurations are possible as well: a_0, $a_0 + a_1$, $a_0 + a_2$, a_3, $a_2 + a_3$. For each one of the cases listed

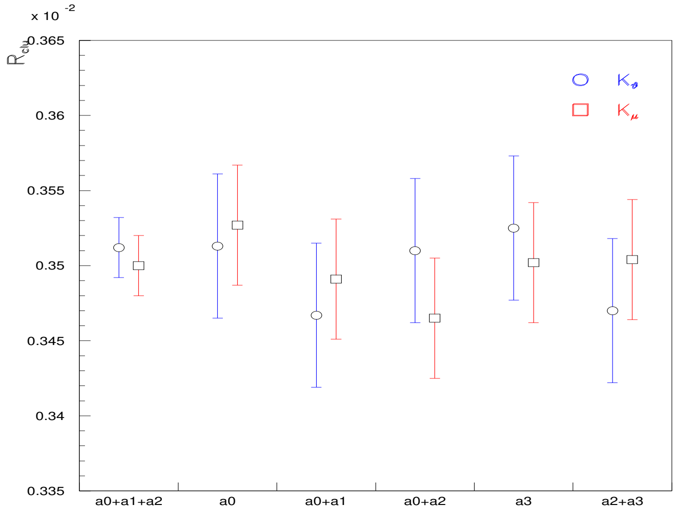

Figure 27: The ratio R_{clu} for different definitions of "*neutral*" clusters (see text). Circles and squares represent the K_θ and the K_μ tags, respectively.

above, the ratio

$$R_{clu} = \frac{N_{tag}^{\tau'}}{N_{tag}} \cdot \frac{1}{\epsilon_{4onT}} \tag{6.1}$$

which determines the final value of the BR, is plotted in Fig. 27, in both the tags hypotheses. The variation of R_{clu} has been included in the total systematic uncertainty quoted for the clustering efficiencies.

The threshold cluster energy has been moved from 13 to 17 MeV, and the maximum value for $|\Delta t'_{jk}|$ has been varied in the interval covered by 4 ± 1: in Fig. 28 $N_{tag}^{\tau'}/N_{tag}$ and ϵ_{4onT} are plotted as functions of these two quantities. Vertical axes are homogeneus and are defined in such a way to overlap in correspondence of the cut specifically used in the analysis.

As a result, the variation produced on R_{clu} is at most $\sim \pm 0.5\%$.

The study of the stability of $BR(\tau')$ with respect to the definition of the procedure of splitting recovery [17] provides a systematic effect of about 10^{-4} on R_{clu} (corresponding to a $\sim 0.2\%$ relative uncertainty).

[17] The parameters r_0 and E_{sup} in (2.6) are varied in the intervals (1000 ± 500) cm and (40 ± 20) MeV.

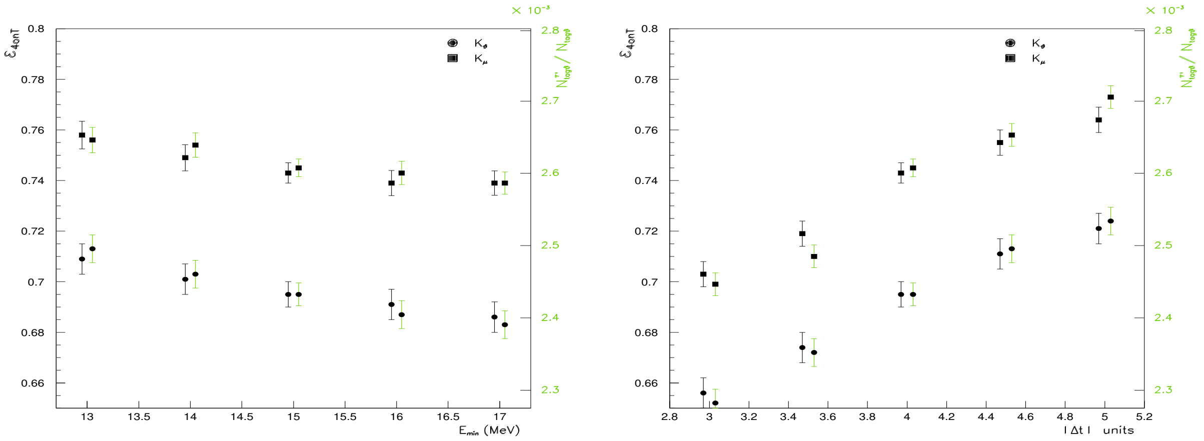

Figure 28: Behaviour of $N_{tag}^{\tau'}/N_{tag}$ (dots with green bars) and ϵ_{4onT} (dots with black bars) when the cuts on the minimum cluster energy (left) and on the maximum value of $|\Delta t'_{jk}|$ (right) are modified. Two shapes can be distinguished for K_θ and K_μ tags, respectively in the lower and higher part of the plots.

6.2 Cosmic veto effect

Cosmic ray events are identified by the trigger [12] directly during data acquisition; the topology in this case is given by two *cosmic sectors* hit in the EMC, *i.e.* sectors where a $\sim 30\ MeV$ threshold for the energy deposit and a suitable time configuration are found in agreement with the hypothesis of a cosmic ray passing through the detector.

In order to quantify the effect of the cosmic veto on the present analysis, the selection algorithm has been applied on the event rejected by the veto. The corrective factor Λ_{CV} has been defined as:

$$\Lambda_{CV} \equiv \frac{\epsilon_{CV}^{\theta,\mu}}{\epsilon_{CV}^{\tau'}} = \frac{1 - \lambda_{CV}^{\theta,\mu}}{1 - \lambda_{CV}^{\tau'}} \ ,$$

where λ_{CV}^{θ} and λ_{CV}^{μ} are the fractions of reconstructed and vetoed events in which a K_θ or K_μ decay has been tagged and self-triggered, and $\lambda_{CV}^{\tau'}$ is the fraction in which also a τ' decay was present in the opposite hemisphere.

λ_{CV}^{θ} and λ_{CV}^{μ} are measured with a good accuracy from data samples C and D:

$$\lambda_{CV}^{\theta} = (8.2 \pm 0.4) \cdot 10^{-4} \quad , \quad \lambda_{CV}^{\mu} = (1.15 \pm 0.03) \cdot 10^{-3} \ , \tag{6.2}$$

while

$$\lambda_{CV}^{\tau'} = (1.2 \pm 0.1) \cdot 10^{-3} \ ,$$

is measured from vetoed data without requiring a tag (to gain in statistics) and rescaled to take into account the increase in the probability to simulate a cosmic when a tag (K_θ or K_μ) is required.

The final correction on $BR(K^\pm \to \pi^\pm\pi^0\pi^0)$ resulting from the cosmic veto effect is

$$\Lambda_{CV} = 0.999 \pm 0.001 \ . \tag{6.3}$$

valid for both tags. In (6.3) the variations of the downscaling factor along the 2001-2002 data acquisition, have been taken into account. The result obtained from Monte Carlo is compatible within errors.

6.3 FILFO algorithm effect

A suitable sample of events rejected by the FILFO algorithm [16] has been used in order to evaluate the probability $(1 - \epsilon_{FILFO})$ that a K_θ/K_μ selftag event is discarded by the FILFO algorithm. The result obtained for ϵ_{FILFO} on data differs from the unity by less than 10^{-3}, but there are no evident reasons why FILFO should introduce a bias in the ratio $N_{tag}^{\tau'}/N_{tag}$ rejecting more/less tagged events containing a τ' than those with other decays. Compatible results are observed on Monte Carlo.

For these reasons the FILFO effect has been considered negligible and no corrections have been applied on $BR(\tau')$ (*i.e.* $\epsilon_{FILFO}^{\theta,\mu}/\epsilon_{FILFO}^{\tau'}$ in equation (1.7) has been assumed equal to 1).

7 Results and conclusions

The values of $N_{tag}^{\tau'}$, N_{tag} and the other measured quantities involved in the measurement of $BR(\tau')$ are reported in Tab. 9, concerning the K_θ and the K_μ selftag. The efficiencies have been evaluated on different data samples according to what described in Sect. 5, while the measurement of $N_{tag}^{\tau'}$ and N_{tag} has been performed on the A data sample (see Tab. 2).

The stability, within the errors, of the efficiencies reported in Tab. 9 has been examined remeasuring the same quantities in data samples different from the ones assigned. Two separate measurements are performed for the two selftags:

$$BR(K^\pm \to \pi^\pm\pi^0\pi^0)_\theta = (1.766 \pm 0.016_{stat} \pm 0.017_{syst}) \cdot 10^{-2} \ ,$$

$$BR(K^\pm \to \pi^\pm\pi^0\pi^0)_\mu = (1.791 \pm 0.015_{stat} \pm 0.017_{syst}) \cdot 10^{-2} \ .$$

The statistical errors include also the contributions from the efficiencies that scale down with the collected statistics. The statistical correlations between the measurements performed on the same data sample (*e.g.* A for $N_{tag}^{\tau'}$ and ϵ_K, and B for ϵ_v and ϵ_{4onT}) have been taken into account [18].

The final measurement of the branching ratio is obtained as their weighted average value [19] :

$$\boxed{BR(K^\pm \to \pi^\pm\pi^0\pi^0) = (1.781 \pm 0.013_{stat} \pm 0.016_{syst}) \cdot 10^{-2}}$$

[18] In general, given two efficiencies (ϵ_1 and ϵ_2) to be measured on subsamples S_1 and S_2 extracted from the same original sample S, the value of $\epsilon_1 \cdot \epsilon_2$ is computed by averaging its correlated measurement in $S_1 \cap S_2$ with the product of the uncorrelated estimates of ϵ_1 and ϵ_2, obtained in $S \setminus S_2$ and $S \setminus S_1$, respectively.

[19] Statistical and systematic errors have been propagated independently only for quantities used in (1.7) which have been actually estimated separately for the two selftags.

	Sample	**tag**$_\theta$	**tag**$_\mu$
$N_{tag}^{\tau'}$	A	30798 ± 180	52253 ± 230
N_{tag}	A	$(1.275 \pm 0.004) \cdot 10^7$	$(1.992 \pm 0.004) \cdot 10^7$
ϵ_K	A	$0.466 \pm 0.001 \pm 0.002$	
ϵ_{vtx}	B,C,D	$0.539 \pm 0.003 \pm 0.002$	
$\langle A_{clu}^4 \rangle$	A	$0.799 \pm 0.001 \pm 0.003$	
ϵ_{4onT}	B	$0.697 \pm 0.002 \pm 0.004$	$0.745 \pm 0.003 \pm 0.004$
ϵ_{Etot}	A,MC	$0.9947 \pm 0.0006 \pm 0.0012$	
$\epsilon_{sel}^{\tau'}$		$0.1392 \pm 0.0010 \pm 0.0013$	$0.1488 \pm 0.0011 \pm 0.0013$
$\xi_{bckg}^{\tau'}$	MC	0.0075 ± 0.0011	
ξ_{bckg}^{tag}	MC	0.0037 ± 0.0002	0.0021 ± 0.0002
Λ_{CV}	C,D	0.999 ± 0.001	

Table 9: Summary of the quantities involved in the measurement of the branching ratio for the K_θ- and for the K_μ- selftag. The data (or MC) sample used for the measurement is also shown. In the rows where only a number is reported, a single measurement is used for both tags. The uncertainties on $N_{tag}^{\tau'}$ and N_{tag} are statistical only, while those on $\xi_{bckg}^{\tau'}$, ξ_{bckg}^{tag} and Λ_{CV} are systematic (see the text for details).

and is plotted in Fig. 29 together with the experimental measurements of $BR(\tau')$ reported in Tab. 1 and the PDG world fit.

In Tab. 10 all the contributions (both statistical and systematic) to the total uncertainty are summarized.

As a consistency check, the value of the branching ratio has been calculated also on Monte Carlo. In this case all the measurements of the quantities involved in (1.7) have been repeated in the same way as done for real data. From MC the estimate of the branching ratio is found to be

$$\left[BR(K^\pm \to \pi^\pm \pi^0 \pi^0)\right]_{MC} = (1.745 \pm 0.042_{stat} \pm 0.036_{syst}) \cdot 10^{-2} \ , \tag{7.1}$$

in agreement with the value 1.73 [2] used as input in the initial Monte Carlo simulation. The systematic error on MC is larger than the one obtained on data since some of the contributions considered in the analysis scale with the collected statistics, that is much lower for the simulated than on the real data.

Source of uncertainty	Relative error (10^{-3})
$N_{tag}^{\tau'}$ statistics	3.5
N_{tag} statistics	0.2
Charged kaon reconstruction/identification efficiency	5.7
Vertex reconstruction efficiency	6.6
Splitting recovery algorithm	2.3
Four clusters acceptance	3.6
On-time requirement for clusters	5.1
Total energy cut	1.4
Background subtraction	1.1
Cosmic-ray trigger veto	1.0
FILFO algorithm	$\ll 1$
$BR(\pi^0 \to \gamma\gamma)^2$	0.7
Total uncertainty	11.6

Table 10: Summary of all the contributions to the total relative error on the measurement of $BR(K^{\pm} \to \pi^{\pm}\pi^0\pi^0)$.

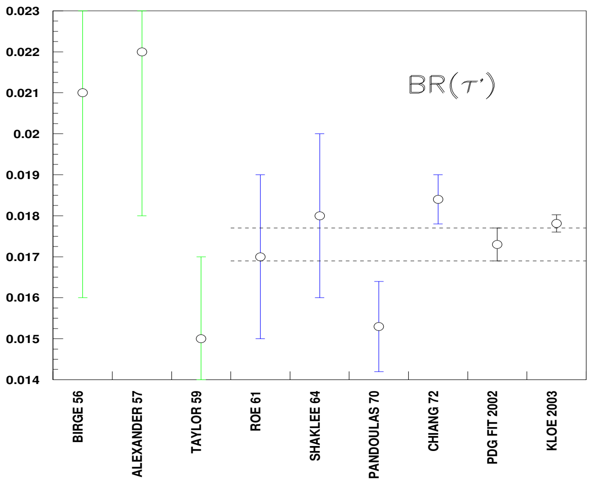

Figure 29: Comparison between the measurement of $BR(\tau')$ obtained in this analysis and the previous world results: the dashed lines delimit the error of the 2002 PDG fit.

References

[1] L. Maiani, N. Paver, *"The second DAΦNE physics handbook"*, INFN, LNF, Vol.1, 51 (1995)

[2] K. Hagiwara et al., *"Review of Particle Physics"*, Physical Review D66, 010001 (2002)

[3] R. W. Birge et al., Nuovo Cimento, Vol.4, 834 (1956)

[4] G. Alexander, R. H. W. Johnston, C. O'Ceallaigh, Nuovo Cimento, Vol.4, 478 (1957)

[5] S. Taylor et al., Physical Review, Vol.114, 359 (1959)

[6] B. P. Roe et al., *"New determination of the K^+-decay branching ratios"*, Physical Review Letters, Vol.7, 346 (1961)

[7] F. S. Shaklee et al., *"Branching Ratios of the K^+ Meson"*, Physical Review, Vol.136B, 1423 (1964)

[8] D. Pandoulas et al., *"Branching Ratios for $K^+ \to 3\pi$ Decays"*, Physical Review D, Vol.2, 1205 (1970)

[9] I. H. Chiang et al., *"K^+ Decay in Flight"*, Physical Review D, Vol.6, 1254 (1972)

[10] V. V. Barmin et al., *Sov. J. Nucl. Phys.*, 48, 1032 (1988)

[11] V. N. Bolotov et al., *Sov. J. Nucl. Phys.*, 44, 68 (1986)

[12] M. Adinolfi et al., *"The Trigger of KLOE"*, Article in press on Nuclear Instruments and Methods in Physics Research, A (2002)

[13] G. Saracino, *"Identification of $\phi \to K^+K^-$ events in KLOE"*, KLOE Memo # 161 (1998)

[14] L. Passalacqua, V. Patera, B. Sciascia, *"$\phi \to K^+K^-$ identification algorithms in KLOE"*, KLOE Memo in preparation

[15] G. Finocchiaro and A. Menicucci, *"Cosmic rays rejection in KLOE"*, KLOE Memo # 203 (1999)

[16] B. Golosio et al., *"Rejection of machine background in the KLOE experiment"*, KLOE Memo # 172 (1998)

[17] M. Incagli, *"VTXFIN: the KLOE Vertex Finder Algorithm"*, KLOE Memo # 147 (1998)

[18] F. Ambrosino et al., *Current status of the track reconstruction using KLOE drift chamber*, KLOE Memo # 177 (1999)

[19] A. Antonelli et al., *Short description of the track reconstruction with the KLOE drift chamber*, KLOE Memo # 194 (1999)

[20] A. Antonelli, C. Bloise, *"The KLOE Monte Carlo GEANFI"*, KLOE Memo 128/98 (1997)

[21] R. Brun et al., *"CERN GEANT3 User's Guide"*, DD/EE/84-1 (1987)

[22] S. Miscetti and T. Spadaro, *"Rate measurement of accidental clusters in the EMC"*, KLOE Memo # 251 (2001)

[23] V. Casavola, E. Gorini, V. Patera, M. Primavera, A. Ventura, *"Machine Background Addition to the KLOE Drift Chamber in Monte Carlo events"*, KLOE Memo # 263 (2002)

[24] M. Antonelli et al., *"The Track to Cluster association program"*, KLOE Memo # 129 (1996)

[25] M. Adinolfi et al., *"The KLOE electromagnetic calorimeter"*, Nucl. Instr. and Methods in Phys. Res. A 482, 363 (2002)

[26] S. Giovannella and S. Miscetti, *"$\phi \to \pi^0\pi^0\gamma$"*, KLOE Note # 178 (2002)

[27] M.Antonelli, L.Passalacqua, B.Sciascia, *"Investigation into the physics of DAΦNE background"*, KLOE Memo # 260 (2001)

[28] H. Fesefeldt, Report PITHA-85/02, RWTH Aachen (1985)